FACULTY
OF MATHEMATICS
AND PHYSICS
Charles University

SUMMARY OF DOCTORAL THESIS

Michal Lacko

Studies of reactions of ions with water molecules in the gaseous phase for trace gas analysis

Department of Surface and Plasma Science

Supervisor of the doctoral thesis: Prof. RNDr. Patrik Španěl, Dr. rer. nat.

Study programme: Physics (P1701)
Study branch: Physics of Plasma and Ionized Media

Prague 2022

MATEMATICKO-FYZIKÁLNÍ
FAKULTA
Univerzita Karlova

AUTOREFERÁT DISERTAČNÍ PRÁCE

Michal Lacko

Studium reakcí iontů s molekulami vody v plynné fázi pro stopovou analýzu

Katedra fyziky povrchů a plazmatu

Vedoucí disertační práce: prof. RNDr. Dr. rer. nat. Patrik Španěl

Studijní program: Fyzika (P1701)
Studijní obor: Fyzika plazmatu a ionizovaných prostředí

Praha 2022

Contents

Abstract / Abstrakt

Chemical ionization mass spectrometry (CI-MS) is a powerful analytical technique, capable to detect trace levels of organic molecules diluted in air samples in real-time. Processes leading to ionization of organic molecules, necessary for their detection and identification, are however often strongly affected by the presence of water vapours in form of sample humidity. In the present work, we studied the influence of water vapours on ion chemistry and, subsequently, the respective influence on sensitivity and selectivity of CI-MS techniques.

Studies were carried out using several soft chemical ionization mass spectrometry instruments, including Selected Ion Flow Tube Mass Spectrometry (SIFT-MS), Proton Transfer Reaction Mass Spectrometry (PTR-MS) and Selected Ion Flow-Drift Tube Mass Spectrometry (SIFDT-MS). Experimental studies were also supplemented by theoretical simulation of proposed ion chemistry using the Kinetic of Ion-Molecular Interaction simulator (KIMI), developed by the author.

In this thesis, we present a study of formaldehyde, glyoxal and phthalates ion chemistry with H_3O^+, NO^+ and O_2^+ reagent ions, focusing on secondary reactions with water vapours. Additionally, we also studied secondary reactions of protonated hydrated acetic acid with acetone. Finally, we have carried out experiments with fast gas chromatography (CG) coupled with the SIFT-MS instrument, to reduce humidity influence and improve the selectivity of monoterpenes.

Metoda hmotnostní spektrometrie pomocí chemická ionizace je účinná analytická technika, umožňující detekovat v reálném čase stopové množství organických těkavých látek přítomné ve vzduchu. Procesy vedoucí ke ionizaci organických molekul, nutné k jejich detekci a následnou identifikaci, jsou bohužel často ovlivněné přítomností vodní páry. V představené práci jsme studovali vliv vodní páry na chemii iontů a její následní vplyv na citlivost a selektivitu metod hmotnostní spektrometrie pomocí chemická ionizace.

Pro studium jsme využili několik hmotnostně-spektrometrických přístrojů, mimo jiné techniku hmotnostní spektrometrie v proudové trubici s vybranými ionty (SIFT-MS), techniku hmotnostní spektrometre pomocí reakce přenosu protonu (PTR-MS) a techniku hmotnostní spektrometrie v proudově-driftové trubice s vybranými ionty

(SIFDT-MS). Experimentální stude je doplněná teoretickými simulacemi studovaných procesů pomocí autorem vytvořením simulačním programem KIMI.

V dizertační práci prezentujeme výsledky zkoumání iontový chemie molekul formaldehydu, glyoxalu a ftalátů pomocí H_3O^+, NO^+ and O_2^+ rekčních iontů, přičemž se zaměřujeme na pochopení sekundárních reakci iontových produktů s vodní párou. Následně jsme taky studovali sekundární reakce protonovaných a hydratovaných molekul kyseliny mravenčí s acetonem. V práci jsme nakonec zkoumali ionizaci monoterpenů kombinací rychlé plynové chromatografie a SIFT-MS, která mimo jiné umožnuje redukovat vliv vodní páry na iontovou chemii.

1. Introduction

1.1. Chemical ionisation of organic molecules

Chemical ionisation is a process achieved through the chemical reaction between ions and molecules. Chemical ionization requires at least two reacting species, A and B, with one of the species carrying a positive or negative charge:

$$A^{+/-} + B \rightarrow products, \tag{1}$$

leading to transfer of charge on the second particle, or eventually initiate atomic rearrangement leading to the formation of new products. The interaction potential between a point ion and spherical molecule at distance *r* was initially described by Langevin [1] as:

$$V(r) = -\frac{1}{4\pi\varepsilon_0}\frac{\alpha q^2}{2r^4}, \tag{2}$$

where q represents the charge of the ion, α is the polarizability of the neutral molecule and ε_0 is the permittivity of the vacuum. For Maxwellian distribution of particle velocities, the ion-molecular interaction potential decreases lead to the temperature-independent Langevin reaction rate coefficient:

$$k_L = \sqrt{\frac{\pi\alpha q^2}{\mu\varepsilon_0}}. \tag{3}$$

This reaction model may however only predict the ion-molecular interaction accurately for atomic ions reacting with small non-polar molecules.

For polar molecules containing permanent dipole moments, the shape of the interaction potential differs. Charge-dipole potential depends on the angle, Θ, between the vector of the permanent dipole moment relative to the mutual orientation of both interacting particles as:

$$V(r,\Theta) = -\frac{1}{4\pi\varepsilon_0}\frac{\alpha\mu_D}{2r^2}\cos\Theta, \tag{4}$$

where μ_D represents the value of the permanent dipole moment of the neutral molecule.

For most ion-molecular interactions, both permeability and permanent dipole moment will be non-zero values. Thus, dipole forces cannot be ignored, and both potentials must be considered. [2] The issue which surrounds modelling is that the mean value

of the relative dipole orientation, Θ, depends on the specific molecular system and differs between molecules in a non-trivial way. Two main approaches have been developed to describe the effect of permanent dipole moments; the average dipole orientation (ADO) theory [3-5] and the parametrised trajectory calculation. [6]

Both theories can be applied to determine collisional rate coefficients, as they only require the available values of polarizability and permanent dipole moment. Nowadays, such values can be easily obtained by using density functional theory (DFT) calculations and thus the collisional rates can be estimated for a large number of molecules. [7]

Thermodynamics of ion-molecular reactions

Based on the thermodynamic properties of reagents, several reaction channels can be observed, as summarized in Table 1. At the low pressures (below 10 mbar), the most important are bimolecular reactions, as they are usually very fast and occur at rates comparable to the collisional rate. Such reactions are very important for chemical ionization as they occur in almost every single collision. Most of them can be supplemented by additional dissociation if the chemical potential is high enough to excite the molecule after ionization (into a repulsive state) and thus overcome the bounding energy which leads to dissociation. Finally, we mainly focus on positive ion reaction, as we have not used negative ions in the present work.

Table 1 List of ion-molecular reactions used for CI.

	Reactants		**Products**	**Condition**
Positive CI				
a,	$A^{+\cdot} + B$	$\rightarrow$	$B^{+\cdot} + A$	$IE(A) > IE(B)$
b,	$AH^{+} + B$	$\rightarrow$	$BH^{+} + A$	$PA(B) > PA(A)$
c,	$A^{+\cdot} + BH$	$\rightarrow$	$B^{+\cdot} + AH$	if exothermic
	$A^{+\cdot} + BR$	$\rightarrow$	$B^{+} + AR$	if exothermic
d,	$A^{+} + B + C$	$\rightarrow$	$AB^{+} + C$	if exergonic
e,	$AL^{+} + B$	$\rightarrow$	$BL^{+} + A$	if exergonic

The first typical process is a charge transfer (Table 1, a), where a cation radical $A^{+\cdot}$ takes an electron from a neutral molecule B, leaving molecule B ionised. The process is exothermic if the ionization energy of neutral B is lower than the recombination energy of the reactant ion, $A^{+\cdot}$. As reactions often occur at thermal conditions, only a negative difference in respective adiabatic ionization energies, $IE(A) > IE(B)$ is required.

An additional process which is very characteristic for CI, is proton transfer (Table 1, b) from a conjugated base (AH^+) to a neutral base (B). The ability of a molecule to bind a proton is represented by its basicity, defined as the negative change of the Gibbs free energy (ΔG) when a neutral molecule accepts a proton. During the reaction, a proton is more likely to be attached to a base with higher associated basicity, while the reaction equilibrium rises with a larger basicity difference. However, as the transfer of a single proton from one base to another does not significantly change the entropy ($T\Delta S$), only the enthalpy change (ΔH) is usually important. The condition for successful proton transfer is for the proton affinity of the neutral molecule (B) to exceed the proton affinity of the neutral (A) currently binding the proton; $PA(B) > PA(A)$. As the proton transfer does not face a potential barrier, the process will be spontaneous after the condition is fulfilled. A series of experiments showed that proton transfer is extremely efficient as the reaction rate almost equals the collisional rate, meaning that a reaction occurs on almost every single collision if the reaction is exothermic by at least 20 kJ/mol. [8]

The next process (Table 1, c**)** indicates a series of different ratio channels, where the reagent ion $A^{+\cdot}$ removes hydrogen or a radical R from the neutral molecule B. The molecule B then remains charged (although with a lighter mass due to the transferred radical, R, or the proton, H). The initial reagent ion becomes neutral as it reacts with the removed fragments. An example of such hydride ion abstractions is found in the reactions of unsaturated hydrocarbon ions with other hydrocarbons, such as $C_3H_5^+ + \text{neo-}C_5H_{12} \rightarrow C_5H_{11}^+ + C_3H_6$. [9]

In addition to hydride ion abstraction, more complex radicals from the neutral may be transferred onto the reagent ion. A typical example of this is found in the transfer of OH^- hydroxide ions which has been observed for alcohols [10] and diols [11]; or

carboxylic acids [12] observed for hydronium (H_3O^+) and NO^+ reagent ions, respectively.

Last but not least, the association (or adduct formation) reaction (Table 1, d), where the colliding particles A^+ and B form a short-lived ion-neutral complex AB^{+*}, is discussed. The complex exists due to the presence of a resonance structure formed by a centrifugal barrier, as the charge can be partially located on both molecules. The complex can spontaneously dissociate back to its original form or be stabilized by the emission of a photon, or more likely in CI, by a collision with a third particle, C. The third particle removes part of the potential energy from the excited transition complex and acquires this energy itself, in the form of kinetic energy. The reaction complex may thus become bounded inside the barrier. The efficiency of the energy transfer during the collision depends on the reduced mass of the complex, as well as on the mass and the number of degrees of freedom of the C particle. The bound energy can be small or significantly high, depending on the type of the reactants defining the enthalpy and the entropy change between the free and bounded states.

Ligand switching (Table 1, e**)** is often not considered as a primary reaction channel, as it cannot proceed from the injected reagent ions. However, the reaction is important for its presence as a secondary process occurring in the ion–molecular system. The reaction often involves neutral or ionised clusters, from which one or more cluster ligands can be transferred to the other reactant. An example of this is when hydronium water clusters [13] react with organic molecules in the system:

$$H_3O^+ + H_2O + He \rightarrow H_3O^+.H_2O + He, \quad (5a)$$

$$H_3O^+H_2O + M \leftrightarrow M.H_3O^+ + H_2O. \quad (5b)$$

The thermochemistry of the process (5b) depends primarily on the different affinity of the transferred ligand (H_3O^+ affinity in the present example). However, as the reaction system contains many molecules, the change in entropy becomes significant. Therefore, describing the reaction only as the difference in particular affinities (otherwise sufficient for proton transfer reactions) is not possible, and the total Gibbs free energy must be considered.

The effect of an external electric field

In the presence of an electric field, ions in the gas phase accelerate along the vector of the electric field, *E*. Collisions with gas molecules cause ions to maintain a mean ion drift velocity, v_d, characterized by ion mobility, μ, as:

$$v_d = \mu E. \tag{6}$$

The ion mobility depends on a collisional cross-section between ions and a buffer gas but is also highly sensitive on gas pressure and temperature.

Increased ion drift velocity has a direct effect on the kinetic energy of the ion and thus on the reaction cross-section. Collisions of ions with neutrals thus do not occur at thermal energies. To describe this effect, we defined the mean collisional energy (KE_{CM}) as the relative kinetic energy available for the reaction process at the centre-of-mass, which is related to the two interacting particles through:

$$KE_{CM} = \frac{m_n}{m_n + m_{ion}}\left(KE_{ion} - \frac{3}{2}k_B T\right) + \frac{3}{2}k_B T. \tag{7}$$

The ion reactions often take place in a system where the analyte molecule is diluted in a buffer (or carrier) gas. The reagent ions thus mainly collide with the buffer gas molecules, while the main interest is to describe the reaction with the analyte. The kinetic energy of the reagent ion is thus characterised by the mass of the buffer gas, m_b, and can be calculated from its drift velocity using the Wannier formula [14]:

$$KE_{ion} = \frac{3}{2}k_B T + \frac{1}{2}m_{ion}v_d^2 + \frac{1}{2}m_b v_d^2. \tag{8}$$

The KE_{CM} can be thus defined for collisions with both buffer gas, $KE_{CM,b}$, and the analyte (neutral reactant), $KE_{CM,r}$:

$$KE_{CM,b} = \frac{m_b}{m_b + m_{ion}}\left(KE_{ion} - \frac{3}{2}k_B T\right) + \frac{3}{2}k_B T, \tag{9}$$

$$KE_{CM,r} = \frac{m_r}{m_r + m_{ion}}\left(KE_{ion} - \frac{3}{2}k_B T\right) + \frac{3}{2}k_B T, \tag{10}$$

where m_r represents the mass of the neutral reactant molecule. The $KM_{CM,b}$ is related to the internal excitation of the reagent ions. An increase of the $KM_{CM,b}$ over the thermal energy causes a redistribution of the rotational and vibrational equilibrium into energetically higher states, resulting in a change in ion reactivity. The $KM_{CM,r}$ then represents the translational collision energy of the reagent ion with the analyte.

Assuming Maxwellian ion velocity distribution, we can define an effective temperature of the system, T_{eff}, as:

$$\frac{3}{2}k_B T_{eff} = KE_{ion} = \frac{3}{2}k_B T + \frac{1}{2}m_{ion}v_d^2 + \frac{1}{2}m_b v_d^2. \quad (11)$$

Thus, T_{eff} is the kinetic temperature corresponding to three degrees of freedom in the centre-of-mass system of the ion and reactant molecule, where the first term represents the thermal energy; the second term represents the energy absorbed from the field which is converted into the ion drift motion; and the last term represents the energy of random motion from collisions with gas molecules. [15, 16] This assumption allows us to simplify the reaction rate function from $k(T, E, p)$ to $k(T_{\text{eff}})$.

Looking back at the Langevin reaction rate coefficient, k_L, (Eq. 3), we see that it is temperature independent. Thus, the collisional rate of non-polar molecules is not affected by elevated collisional energy. For polar molecules, the ADO theory predicts the temperature dependence as $T^{-1/2}$. Su [17] also developed a parametric representation of the ion-polar molecular collision rate for kinetic energy dependence. In conclusion, all theories predict the reduction of the collisional reaction rate for polar molecules, as KE_{cm} increases as a function of $T_{eff}^{-1/2}$, or eventually with a slightly faster reduction when also considering higher orders of Eq. 11.

The reaction rate however differs from the collisional rate and the dependence on KE_{cm} and T_{eff} changes with the type of reaction. Multiple studies can be found investigating ion molecular reaction rates under variable electric fields, or more frequently, under variable gas temperatures. [18-20] Also, reactions shall be divided into several sub-categories, reflecting the different natures of ion-molecular reactions which include whether the reaction is exothermic or endothermic; slow or fast (compare to collisional rate); unimolecular or bimolecular; and if ions react with non-polar or polar neutrals.

To summarize, the reactions are affected not only by elevated translation energy of reacting ions but also via the internal rotational and vibrational excitations resulting from their frequent collisions with the neutral buffer gas. The significance of such excitations and the translational energy for ion molecular interactions has to be evaluated individually for every reaction, as it differs depending on the reactants and buffer gasses. In the context of chemical ionization for trace gas analysis, the application of an electric field has the following consequences:

1, The reaction rates for the main ionization processes (charge transfer and proton transfer) are affected only slightly. However, for increased collisional energies a new dissociation channel may open, producing ion fragments. [21, 22]

2, Slow ion molecular reactions will have their reaction rates reduced following the power-law decay. However, for higher collisional energies the internal excitation of the reagent ion may change the character of the reaction resulting in the reaction becoming fast and thus significant. [21, 23]

3, Ligand switching reactions (when slow) also undergo a negative energy dependence.

4, The reaction rate for association reactions also follows the power-law decay. Additionally, the formed ion complex is usually weakly bounded. Therefore, a reversed collisional-induced dissociation reaction reduces the abundance of the associated complexes, even more. Thus, for collisional energies above the cluster bound energy, the abundance of ion clusters decays much faster. [24]

5, The energy dependence of reaction rate for slow ion molecular reactions cannot be directly compared with the thermal dependence obtained in thermalized experiments.

6, For collisional energies at around 1 eV and above, slow reactions are no more visible as collisional-induced dissociation. Dissociative charge transfer and dissociative proton transfer reactions dominate over other reaction channels.

1.2. Analytical techniques for trace gas analysis

Selected ion flow tube mass spectrometry (SIFT-MS)

The SIFT technique was developed in 1976 by Adams and Smith [25] and quickly became the standard in the study of ion-neutral reactions, near to thermal interaction energies [26]. For analytical applications, the SIFT technique was implemented into the SIFT-MS instrument. The instrument consists of four main parts: a discharge generating reagent ions; a mass filter selecting one specific ion; a flow tube where selected ions react with gasses in the presence of a carrier gas; and finally, a mass spectrometer at the end of the flow tube. In the present work, we used a SIFT-MS Profile 3 instrument (see Fig. 1) developed by Instrument Science, Crewe, UK.

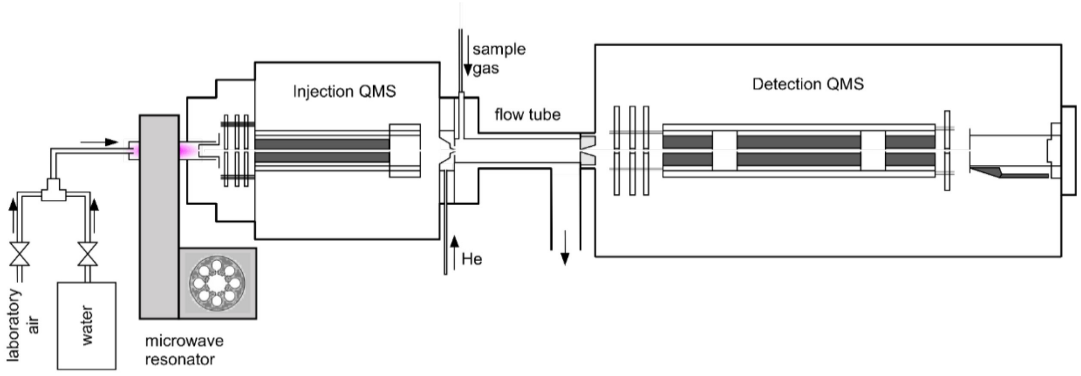

Figure 1 The schema of SIFT-MS experiment. *QMS* - quadrupole mass filter

The SIFT-MS uses a microwave discharge usually within a mixture of water vapour and air. The combination of both gasses allows for the formation of several stable ions, mainly H_3O^+, NO^+ and O_2^+ which may be used in analytical applications. From the discharge, ions are selected according to their *m/z*, first by a quadrupole mass filter; subsequently by a series of electrostatic lenses focused into the centre of a Venturi-type orifice; and injected into the flow tube. In the flow tube, reagent ions are mixed with helium and are carried along by the carrier gas stream through the flow tube. At typical conditions (300 K, 1 mbar), the laminar flow distribution is established, while ions are mostly concentrated in the centre of the stream. A gaseous sample is introduced through the inlet into the centre of the helium gas 1 cm downstream from the injection orifice, where they are mixed with the carrier gas and reagent ions. From this point, the mixture of all components travels to the end of the flow tube, (4 cm from the sample inlet). During this transport, the reagent ions react with the neutral molecules at a defined pressure and temperature. At the end of the flow tube, ions are sampled through the exit orifice into the quadrupole mass spectrometer and are detected by a Channeltron detector.

The neutral number density of the analyte [M] may then be calculated from the corresponding ion count rate [27] as:

$$[\mathrm{M}] = \frac{1}{t_r} \frac{f_{p1} {I_{p1}}/{D_{ep1}} + f_{p2} {I_{p2}}/{D_{ep2}} + \cdots}{f_{i1} I_{i1} k_1 + f_{i2} {I_{i2} \frac{k_1 + k_2}{2}}/{D_{ei2}} + \cdots}, \tag{12}$$

where I_{p1}, I_{p2}, etc. correspond to the count rates of individual product ions corrected for mass discrimination, I_{i1}, I_{i2}, etc. represent the count rates of individual reagent ions reacting with M. k_1 and k_2 are the reaction rate coefficients for the main and secondary reagent ions, respectively. D_{ep} and D_{ei} are the respective differential diffusion enhancement coefficients, and t_r is the reaction time. Finally, the auxiliary factors f_p and f_i correct for the calculation of non-linear reaction kinetics.

The concentration of the trace gas in the sampled air may be determined from the previously calculated number density [M] if both the sample gas flow (Φ_s) and carrier gas flow (Φ_c) are carefully measured. The concentration, C, may then be calculated as:

$$C = [\mathrm{M}] \frac{k_b T_g}{p_g} \frac{(\Phi_c + \Phi_s)}{\Phi_s}, \tag{13}$$

where k_b is the Boltzman constant, p_g represents the total pressure of the carrier gas and T_g is the gas temperature. One may directly calculate the relative concentration of the trace gas as p_M/p_0, using Loschmidt`s number ($n_0 = 2.687 \times 10^{19}$ cm^{-3}) which represents the reference concentration at standard atmospheric pressure (p_0 = 1,013.25 mbar) and temperature (T_0 = 273.15 K):

$$\frac{p_M}{p_0} = [\mathrm{M}] \frac{p_0}{n_0 p_g} \frac{T_g}{T_0} \frac{(\Phi_c + \Phi_s)}{\Phi_s}. \tag{14}$$

The calculated concentration may be converted into the commonly used parts-per-million (ppm) or parts-per-billion (ppb) units, by multiplying by 10^6 or 10^9, respectively.

Proton transfer reaction mass spectrometry (PTR-MS)

The PTR-MS (see Fig. 2) is a technique developed by Lindinger et al. [28], based on discoveries obtained by the FA and SIFT. The instrument is tuned to provide a highly sensitive analysis of various organic compounds in real-time with a high level of resolution. Three major upgrades were conducted to achieve such properties which were: an absence of an injection mass filter allowing for a high ion flux of reagent ions; secondly, the absence of a carrier gas but with the full volume of the reaction chamber being filled with the sample gas; and finally, the introduction of an axial homogenous electric field (drift tube) accelerating ions through the reaction region

into the detecting mass spectrometer (while increasing the reaction energy of each ion-molecular reaction).

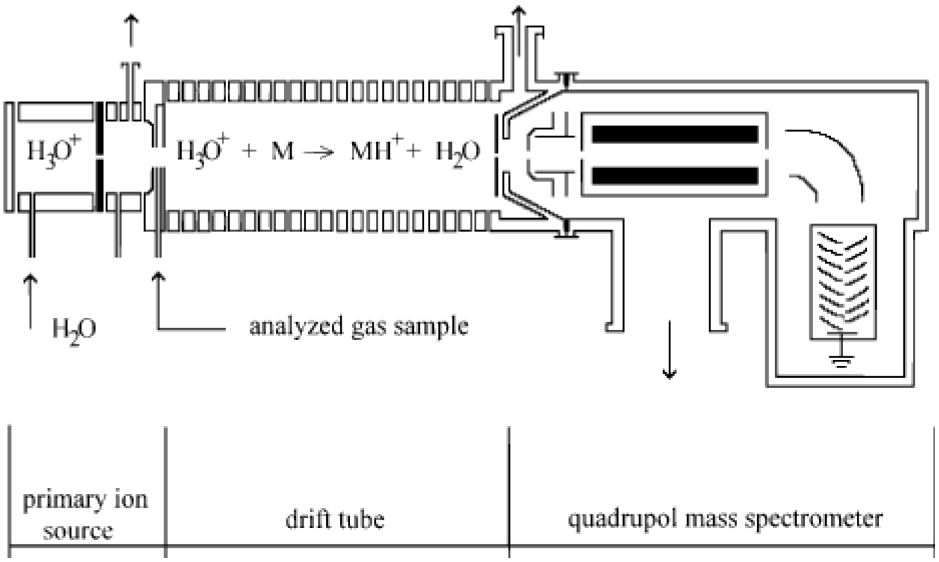

Figure 2 A scheme showing the PTR-MS instrument. [144]

For the ion source, PTR-MS often uses a DC hollow cathode discharge. The plasma in the discharge is generated in pure water vapour at pressures of around 1 mbar, producing a flow of hydronium ions. The ions formed in the discharge pass through a pin hole which introduces them to the next separation chamber followed by the drift tube. Ions introduced into the drift tube are immediately accelerated along the central axis of the drift tube. The PTR-MS operates at a pressure of around 2 mbar. The sample inlet is placed at the beginning of the drift tube, where the inlet gas may effectively mix with the reagent ions.

A characteristic parameter used in PTR-MS is the reduced strength of the electric field, *E/N*, accelerating ions along the drift tube. This value is calculated from the drift tube length, *d*; applied electric potential across the drift tube, ΔV; and the pressure of the analysed sample gas in the drift tube:

$$\frac{E}{N} = \frac{\Delta V}{Nd}, \text{where } \left[\frac{E}{N}\right] = \text{V.m}^2 \text{ and } 1\ \text{Td} = 10^{-21}\ \text{V.m}^2. \quad (15)$$

The number density of the sample gas, N, is defined as:

$$N = \frac{N_A}{V_M}\frac{273.15}{T_d}\frac{p_d}{101.325}, \quad (16)$$

where N_A is Avogadro`s number (6.022 x 10^{23} mol^{-1}); V_M is the molar volume of an ideal gas at a temperature of 273.15 K and a pressure of 1 atm (101.325 kPa); T_d is the drift tube temperature; p_d is the drift tube pressure. The E/N used in PTR-MS ranges from 80 Td to 300 Td, depending on the instrument. The most widely used value (and often used as the reference) of E/N is 130 Td.

The concentration of analyte [M] can be determined from the detected ions signals, $i(MH^+)$ and $i(H_3O^+)$, as:

$$\frac{[MH^+]\mu_{0,MH^+}}{[H_3O^+]\mu_{0,H_3O^+}} = \frac{i(MH^+)\mu_{0,MH^+}}{i(H_3O^+)\mu_{0,H_3O^+}} = k[M]t_d, \quad (17)$$

where k represents the reaction rate constant; $\mu_{0,H3O+}$ and $\mu_{0,MH+}$ are the reduced field-dependent ion mobilities of H_3O^+ and MH^+ ions. To determine the concentration of the analyte, we need to know the transition properties of individual ions. In most situations, however, the instrument must be calibrated to obtain transition ratio coefficients for individual substances. [29] Once obtained, the absolute concentration of analyte ion in the sampled gas may be calculated.

Even though the presence of an electric field complicates the determination of the absolute analyte concentration, it is a necessary part of the instrument due to the high concentrations of H_2O vapour present in the discharge and the drift tube, forming hydrated hydronium ions $H_3O^+(H_2O)_n$, where n >1. As water clusters are usually weakly bounded. For increasing E/N the equilibrium quickly shifts towards higher concentrations of H_3O^+ (see Fig. 3). Increasing E/N to higher values is beneficial for a greater distribution of hydronium hydrates, however, this also causes negative secondary effects. Therefore, in most applications, E/N ~ 130 Td is chosen as a compromise between having a sufficient reduction in hydronium hydrates concentration (abundance of $H_3O^+H_2O$ around 10% of H_3O^+ intensity); and fragmentation induced by electric field, of an insignificant level.

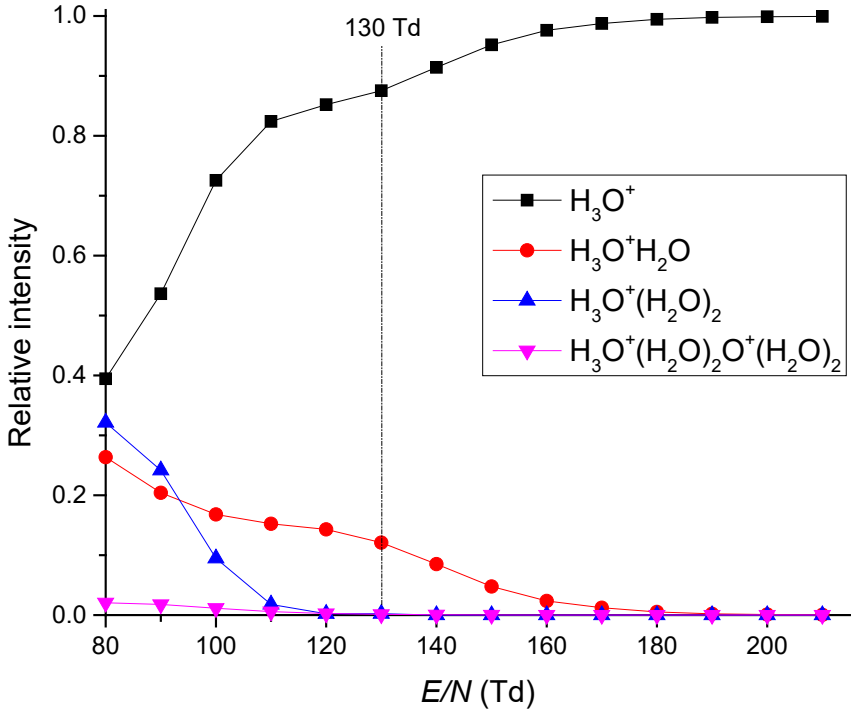

Figure 3 Relative intensity of hydrated hydronium clusters $H_3O^+(H_2O)_n$, n = 0,1,2,3 in PTR-MS determined for various *E/N* values for a sample containing 0.6% humidity (absolute).

Selected ion flow-drift tube mass spectrometry (SIFDT-MS)

SIFDT-MS is a compilation of both PTR-MS and SIFT-MS, exploiting the strengths of both instruments. SIFDT-MS is equipped with an injection mass filter, allowing for a specific reagent ion to be selected. Selected ions are then injected into a flow-drift tube reactor. Flow-drift tubes use helium carrier gas in combination with an axial electric field, reducing diffusion losses to the walls as well as pumping speed requirements. The abundance of primary ion hydrates in the carrier gas in SIFDT-MS is lower compared to PTR-MS. Therefore, the *E/N* used in the SIFDT-MS reactor is lower than in the PTR-MS reactor. In the present work, we used a SIFDT-MS instrument developed by Spesyvyi et al. [24] This instrument additionally contains the possibility to directly determine the ion retention time via the application of a

modulated signal on the injection ion optics. This therefore allows for the acquisition of ion mobilities and reaction energies data.

For SIFDT-MS used in this work (see Figure 4), the reagent ions are generated in a glowing cathode discharge, operating in a water vapor/synthetic air mixture. After extraction from the discharge, reagent ions are introduced via ion optics into the quadrupole mass filter. Ions with selected *m/z* are injected into the transition ion optics, equipped by the shutter grid. The shutter grid can modulate the ion transmission by applying the Hadamard modulation. [30] From the transition ion optics, ions are injected into the flow-drift tube (as a continuous stream or modulated by Hadamard modulation). The drift tube reactor is 145 mm long. In the flow-drift tube, ions are carried along the tube by a homogenous electric field in a ~150 sccm reverse flow of He (1.5 mbar and 24 °C). Application of the voltage along the resistive layer (100 to 500 V) creates a homogenous electric field (from 10 to 100 Td) inside the cylinder. At the end of the flow-drift tube, ions are introduced via an orifice into the quadrupole mass spectrometer and are detected by the electron multiplier with conversion dynode. Sample gas is introduced into the helium gas stream at the end of the flow-drift tube and is carried through in helium flow reverse to the ion movement.

During the study, the SIFDT-MS instrument was frequently modified. A notable improvement as a result of this study was in the modification of the ion source. [31] In the modification, a hollow cathode discharge operating in a water vapor/synthetic air mixture produces primary reagent ions. Ions are then transferred through to the stacked ring ion guide (SRIG) housed in a polypropylene vacuum chamber, operating in helium buffer gas (5.3 mbar), where they thermalize. Thermalized ions carried by the electric field and helium flow enter the next chamber (with a 50 mm long octupole), with an He pressure of about 0.3 mbar. Using an octupole, ions are guided through an aperture into the quadrupole mass filter. Filtered ions are introduced via the Venturi inlet to the small flow-drift tube (VDT in Figure 5), where ions are mixed with He buffer gas and thermalized again. At the end of the VDT, a series of three meshes are present which are required for Hadamard modulation of the ion current.

The second design was built to generate a wider spectrum of reagent ions. The octupole chamber is equipped with a separate gas inlet. The gas molecules then react with

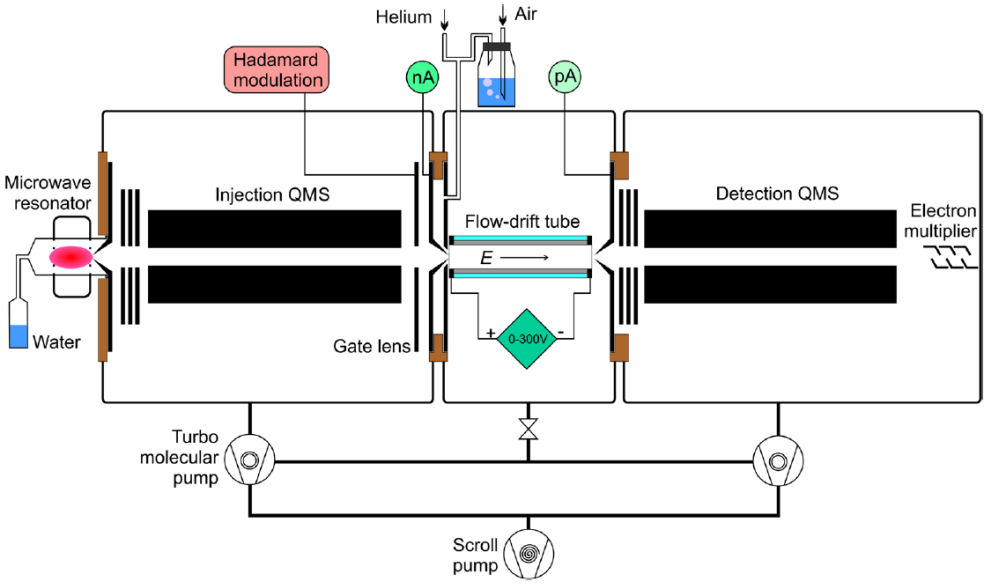

Figure 4 The SIFDT-MS instrument; the initial concept. [24]

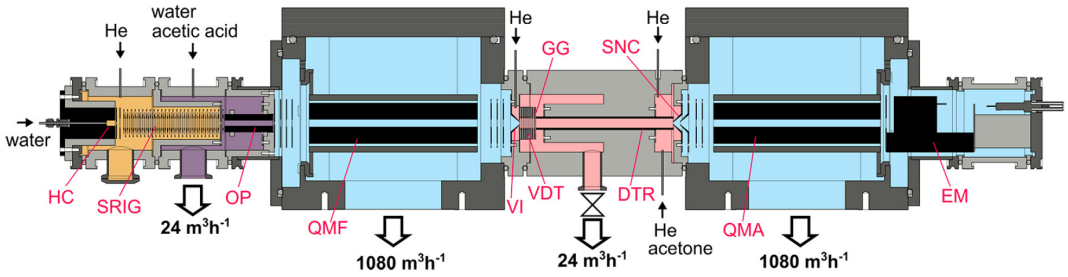

Figure 5 The SIFDT-MS instrument; the final design. [31] The coloured areas represent individual pressure regions: 5 mbar (yellow), 0.3 mbar (violet), 5×10^{-6} mbar (blue), 1.9 mbar (pink). HC - hollow cathode ion source, SRIG – stacked ring ion guide, OP - octupole, QMF - quadrupole mass filter, VI - Venturi inlet, VDT - Venturi flow-drift tube, GG - gating grid, DTR - drift tube reactor, SNC - ion sampling nose cone, QMA - quadrupole mass analyser, EM - electron multiplier with conversion

primary reagent ions and become ionized via CI, for example via proton transfer from hydronium hydrates. The newly formed ions may be then introduced into the flow-drift tube via a quadrupole mass filter. This instrumental design allows for the generation of several various ions, allowing for a more in-depth study of particular (mainly secondary) reaction channels.

1.3. Areas of application

In previous sections, we have compared some aspects of SCIMS techniques and the reference technique, GC-MS. Now, we should discuss the benefits of SCIMS related to analytical applications, mainly high sensitivity, selectivity and rapid response time.

Probably the most notable area of application is analysis of human breath. As breath is exhaled through alveoli in lungs (in direct contact with the blood stream) there is potential for obtaining valuable clinical data using a non-invasive approach. For a decade, researchers have been analysing the potential of breath analysis within clinical applications, identifying several characteristic metabolites presented in human breath: ammonia, acetone, methanol, ethanol and isoprene. [32-35] Most typical is the analysis of acetone (as a direct metabolic product) for type 2 diabetes. [36] Targeted analysis and quantification of acetic acid may be used for monitoring patients with gastroesophageal reflux disease. [37] A promising application is the monitoring of VOCs emitted from bacterial infection [38-41] related to cystic fibrosis - autosomal recessive disorder affecting mainly children. [41, 42] This non-invasive approach was also used for the monitoring of advanced chronic kidney disease [43, 44] and chronic liver disease [45, 46]. Asthma is an additional disease which may also be diagnosed by SCIMS. [47, 48] Interestingly and promisingly, it is possible to analyse n-pentane with this method; a metabolite produced from inflammation within the body which may be a valuable in the diagnosis of chronical Crohn's disease. [49, 50] A big effort has been made to find a biomarker for lung cancer diagnosis, however, little success has been gained so far. [51]

SCIMS techniques are also highly used in environmental applications. They are used in the identification and monitoring of biogenic VOCs (mainly monoterpenes) emitted from various ecosystems. Several studies were carried out investigating emission cycles in tropical rainforests [52-54], coniferous forests [55-57], deciduous forests [58-60], plantations [61-64], grasslands [65-67] and many more. [68, 69] Atmospheric chemistry is a topic directly related to global warming. Studies related to investigating emissions from rural and livestock activities; [70-72] the marine environment including bio-emissions of sea floor [73-75]; as well as industrial contamination; are of significant importance [76, 77].

Besides natural sources, atmospheric chemistry is heavily influenced by anthropogenic emissions which are also frequently studied and monitored by SCIMS. In the urban environment (mainly big cities) VOCs like isoprene, benzene and toluene together with NO_x are an important source of pollution via the production of ground-level ozone. The concentration of VOCs, as well as their secondary products during daytime hours have been investigated in many big cities including Houston [78], Barcelona [79], Tokyo [80], Paris [81, 82] and more. [83, 84] Related research focuses on individual sources of pollutants, such as diesel [85] and aircraft engine emissions [86, 87], as well as industrial sources [88, 89]. Besides outdoor air quality, indoor air quality studies focus on various emissions present in indoor environments. This includes the study of volatiles released from the use of everyday domestic products [90-92], wall paintings [93] and building materials [94].

The final significant application of SCIMS is homeland security and detection of warfare and threat agents. This includes the detection of drugs, explosives or others dangerous chemicals. [95-98] The detection of explosives is dominated by IMS systems, achieving very low detection limits (even though explosives are known for their low volatility). [99] By using PTR-MS, however, much better selectivity of individual explosives may be achieved. [100-102] SIFT-MS is used by customs offices in New Zealand and Canada to screen the shipping containers for the presence of toxic chemicals (fumigants) which may endanger staff during container inspection. [103]

1.4. Limitations of chemical ionization mass spectrometry

The applicability of SCIMS techniques for analytical applications is limited by two main factors: sensitivity and selectivity. Sensitivity describes the minimal concentration of trace gas in the analyte at which the SCIMS instrument is able to determine its presence (and quantify the analyte concentration) with respect to the background noise. Selectivity represents the ability of instruments to distinguish individual analyte components as well as determine their exact molecular composition. The aim of SCIMS instruments is to optimise both sensitivity and selectivity, without losing any of the benefits of using SCIMS. This is namely the use of pre-concentration systems and chromatography affecting the calibration requirements and rapid detection possibility, respectively.

The sensitivity of SCIMS is mainly determined by the design and type of instrument. The new generation of instruments is reaches detection limits up to ppt/ppq levels. This is mainly due to the advanced design of transfer ion optics and their implementation in the drift tube.

Selectivity on the other hand is mainly determined by ion chemistry occurring inside the SCIMS reactor, as well as by the resolution of the mass spectrometer. The characteristic feature of chemical ionization is the formation of product ions which carry information about the mass of the neutral reactant (M), by formation of M^+, MH^+, $M\text{-}H^+$, … ions. This however also occurs for isobaric and isomeric molecules which thus cannot be easily distinguished. With increasing molecular mass, the number of isobaric compounds increase. Both main analytical SCIMS instruments (SIFT-MS and PTR-MS) use different approaches to resolve isobaric molecules. SIFT-MS uses a combination of multiple reagent ions (H_3O^+, NO^+ and O_2^+) that may be selectively introduced into the flow tube. Different types of molecules, producing similar ion products using one reagent ion, tend to react differently with other one. PTR-MS instruments are equipped high-resolution Time-of-Flight mass spectrometry (ToF-MS, resolution power > 10.000), able to differentiate between isobaric molecules.

The concentration of water vapour in a sample gas depends on the sample sources and may vary from few ppm in an extremely dry sample gas, up to tens of thousands of ppm in gases saturated by water vapour. The pressure of a gas which is saturated with water vapour is very temperature sensitive. In breath analysis, the water concentration of a healthy patient with a body temperature of 36 °C is about 5%. Similar concentrations are seen in tropical forests. At room temperature, the absolute humidity may vary from 1% to 2.5%. The level of water vapour within a sample is important as this directly affects the selectivity and sensitivity of analysis, via a series of secondary reactions:

1, Association reaction with primary ions

All three primary reagent ions, H_3O^+, NO^+ and O_2^+ associate with H_2O forming ion hydrates. In SIFT-MS, for NO^+ and O_2^+, mostly $NO^+.(H_2O)_{1,2}$ and $O_2^+.(H_2O)_{1,2}$ hydrates are seen in the spectra. However, for H_3O^+, much larger hydronium hydrates may be observed, up to $H_3O^+.(H_2O)_4$. In PTR-MS and SIFDT-MS the formation of hydrates is reduced, however not completely removed. The presence of reagent ion

hydrates not only reduces the selectivity of the instrument by interfering with product ions with similar *m/z*, but also reduces the concentration of primary reagent ions (which in turn reduces sensitivity of analysis), for samples with higher humidity.

2, Secondary reactions of reagent ion hydrates

Reagent ion hydrates, formed via the association reaction of H_2O and the buffer gas, may often also react with the studied analytes. However, the products of these reactions may not correlate with the primary reaction channels. The possibility of protonated hydronium hydrates to initiate proton transfer is reduced, as proton affinity of water clusters increases with cluster size. [104] A similar reduction in this reactivity applies for the charge transfer process initiated by NO^+ and O_2^+ as well as their respective hydrates. Moreover, reagent ion hydrates often react via ligand switching, forming hydrates of analyte ions:

$$H_3O^+.(H_2O) + M \rightarrow H_3O^+.M + H_2O. \quad (18)$$

This increases the number of analyte ion products.

3, Secondary reactions of analyte product ions

Product ions also interact with water vapour, forming ion hydrates via a three-body association reaction, in the same way as primary ions:

$$MH^+ + H_2O + N \rightarrow H_3O^+.M + N. \quad (19)$$

The level of hydration is dependent on the size and molecular structure of the primary ion, hydration level as well as on other parameters as gas temperature and gas pressure. Some molecules do not form hydrates (i.e. monoterpenes [105]) whereas others form hydrates very effectively (i.e. ketones or alcohols [27]). The ion chemistry is very specific for individual product ion hydrates. The formed product ion hydrates may either be stable; undergo additional reactions with H_2O molecules as reverse ligand switching:

$$MH^+.H_2O + H_2O \rightarrow H_3O^+.H_2O + M, \quad (20)$$

as well as undergo a chemical reaction producing unique ions.

The final reaction pattern is a combination of primary ionization reactions in conjunction with all associated secondary reactions. The influence of individual secondary processes differs for individual reagent ions as well as for different analytes.

To illustrate this complexity, Fig 6 shows a full reaction diagram considering all primary and secondary reactions for the reaction between H_3O^+ with a neutral reactant, M, in the presence of water vapour.

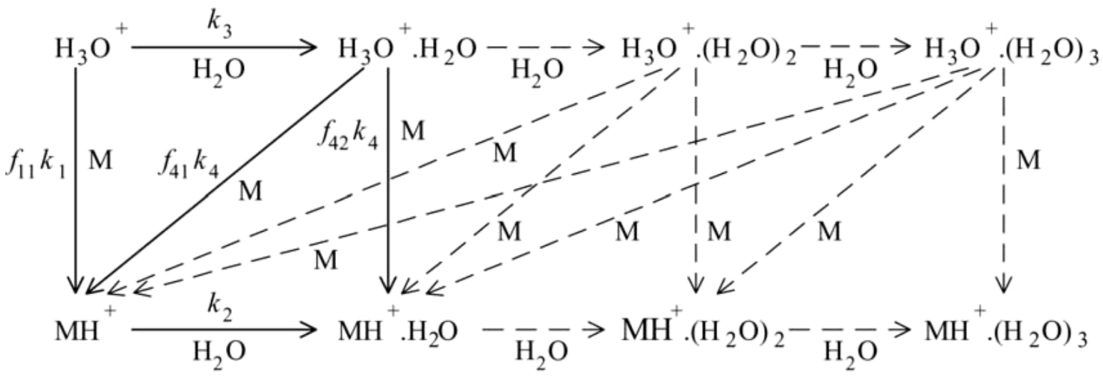

Figure 6 Illustrative reaction diagram of primary and secondary reactions of H_3O^+ with neutral a reactant, M, in the presence of water vapour. [106] Solid line reactions represent moderate humidity levels. Dashed reactions represent saturated water vapour.

In conclusion SCIMS ion chemistry uses main ionization reaction channels (first order approximation) to determine the concentration of selected analytes. The presence of secondary reactions, however, induced mainly by water vapour increases the amount of ion products, affecting both sensitivity and selectivity of the analysis. Therefore, for humid samples or environments with rapidly changing humidity, it is also essential to consider the secondary reaction channels and include secondary ion products into the concentration calculation. Thus, careful understanding and analysis of secondary reaction channels is necessary.

2. Construction of fast GC pre-separation for SIFT-MS

Identification of specific isomers in SCIMS is difficult. Isomers (especially structural isomers) react in a similar way with all reagent ions and thus it is difficult to identify them using multiple reagent ion approaches or using high-resolution MS. The same problem occurs even in the presence of an electric field. Product branching ratios for isomers may differ even if products have the same *m/z*. In a complex sample with an unknown mixture of different isomers, quantitative analysis is very difficult and sometimes impossible.

A classic method used to analyse the concentration of different isomers is gas chromatography. The different structure of individual isomers affects their interaction with the active phase of the column. Isomers may be then analysed based on different retention times. [107, 108] A difference in retention time is not guaranteed, but a difference in the molecular structure often leads to differences in the retention time. Classical GC analysis is however time consuming. Based on the type of the column and temperature profile of the analysis, one measurement may take up to an hour to run. This is in contrast to SCIMS techniques, which have built their reputation on real-time fast analysis.

To solve the problem of isomer analysis, we need to make a compromise between the speed of chromatography analysis and its quality. Comparing to classical chromatographic techniques, SCIMS does not require the separation of all molecules presented in the sample. Instead, SCIMS aims for a specific isomer presented in breath or environmental samples, as other molecules can be determined by ion chemistry. Thus, the chromatography coupled to SCIMS may be less specific. The modern solution to this problem used in SCIMS analysis is called fast gas chromatography (fast GC).

In this work, we have demonstrated the analytical value the novel combination of fast GC coupled to SIFT-MS. As an enhancement to fast GC systems combined with PTR-MS, we went on to achieve a relatively high LOD (~ 16 ppbv). This is mainly due to the limited sample flow eluting from the column (2-3 sccm) which seems insufficient for SIFT-MS (usually using an order of magnitude more). This could be resolved by using a wider column or by using multiple capillaries in parallel. The use of multiple reagent ions was however a clear advantage as it improved the identification of

individual monoterpenes within the chromatogram which was not fully resolved. Finally, the overall benefit of fast GC (not yet stated) is the successful separation of water vapour from the sample. As we observed, the retention time of water is much faster compared to the retention time of the studied monoterpenes. Water vapour is thus evacuated from the flow tube before the analyte of interest is ionized. Consequently, ion chemistry is not significantly affected by system humidity which allows for a systematic use of product branching ratios in future analyses, regardless of sample humidity. This is a very strong benefit of this technique, improving both selectivity and sensitivity of VOC determination in environmental settings.

The full study describing the coupling of fast gas chromatography to selected ion flow tube mass spectrometry for the analysis of individual monoterpenes within mixtures is presented in [109].

3. Complex model of ion chemistry in SCI-MS

The ion chemistry within the reactor tubes can be very complex. This is because the main ionization channels produce multiple ion products and all main ion reactants and products may react with water vapour in a series of secondary reactions. The presence of secondary reactions increases the complexity of mass spectra, reducing selectivity and sensitivity of the technique. In order to determine the concentration of the analyte, the calculation must consider the ion intensities of all product ions, as well as those produced by secondary reactions. Changes in samples humidity (as well as other components as CO_2) thus affects the presence of secondary ion products. For the successful application of SCIMS in ambient environments where sample humidity may change over time, the secondary reactions must be well understood. For this reason, we have built a numerical simulator capable of simulating the ion chemistry within the reactor flow-tube.

The Kinetics of Ion Molecular Interactions Simulator (KIMI Sim) is a numerical simulator of ion-chemistry found in SCIMS instruments. [110] KIMI was produced to help users understand complex ion-neutral molecule interactions and to simulate the ion and neutral molecule number densities in a flow tube or a drift tube. KIMI may however also be used to simulate various other problems involving ion-molecule

interactions. The software was built as a Windows desktop application in the .NET 4.6.1 framework in C#. KIMI uses an interactive graphical interface where the proposed set of ion-molecular reactions may be created. The KIMI then transforms the graphical reaction into a set of kinetic equations that are solved along the central axis of the reactor tube using the classical Runge-Kutta algorithm. [111] Results of the simulation may then be interactively inspected, downloaded or compared with experimental results. The details of how to access the KIMI software are presented at the end of the thesis, in the Attachment A.7.

The software is composed of two core programs (classes) (see Figure 7). The Main program is responsible for management of software settings; main simulation properties; management of individual reaction species as well as for the interactive graphical interface where the proposed reaction sequence is formed. After definition of all physical properties and the formation of a valid reaction scheme, the main program constructs the calculation, calculating all essential information. Calculation control also allows the user to modify some reaction properties, for example reaction rate constants. Additionally, user may enable a homogenous electric field into the simulation. Furthermore, the calculation control also enables a multidimensional simulation by presenting a range of *E/N* values (or a range of number densities) of one of the reactants. If this option is selected then the simulation will be executed for every value of *E/N* or reactant concentration within the pre-defined range. After initialization of the calculation, the calculation control transforms the reaction objects into a set of differential kinetic equations and solves them along the central axis of the reactor. The calculation is executed by the construction of a "calculation" program, executing a one-step solution (via a differential equation). The process is repeated across selected reaction coordinates. The final data set is stored within a Data management class entity, from where it is accessed through the data plot function. Data plot is also capable of comparing simulation results with experimental data.

The functionality of KIMI was tested on a series of experimental data, produced by SIFT-MS and SIFDT-MS methods. For the initial test, we studied the influence of water vapour concentration on the formation of hydronium hydrates in SIFT-MS. In later work, we conducted similar experiments involving acetone vapours. Both the hydronium reactions with water vapour as well as with acetone are well described in

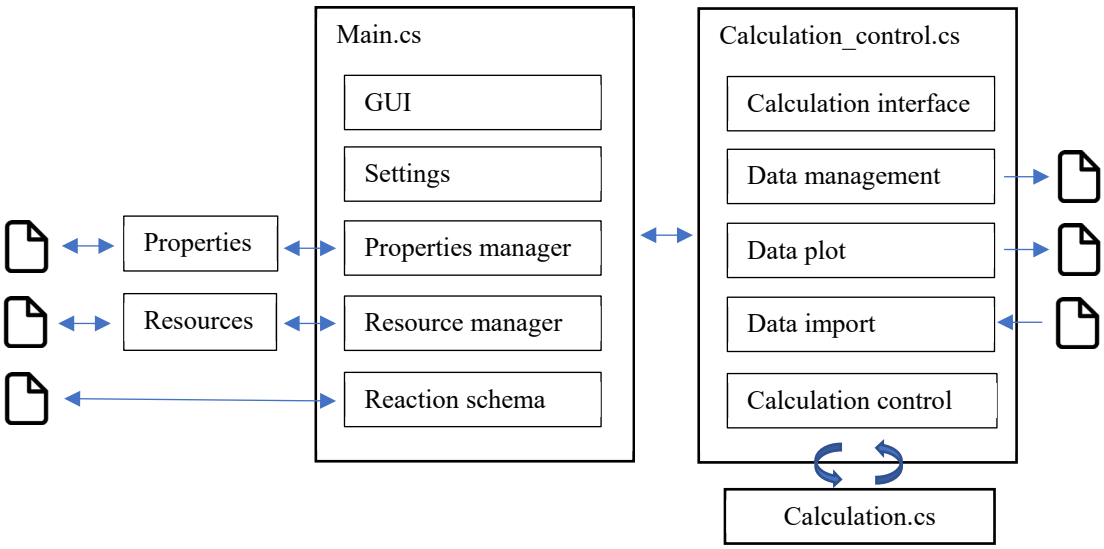

Figure 7 A schematic view of the KIMI main programs and their functionalities.

literature. [112-115] As a result, we used the set of known reaction rate constants as a foundation the for simulation of ion chemistry in the program. Reaction rate constants were subsequently optimised to interpolate experimental data. For the experiment, we used a nalophan bag filled with dry air and acetone for the second study. The humidity of our sample was changed by injecting warm liquid water into the sample bag while the sample gas was introduced into inlet of the SIFT-MS. SIFT-MS is capable of directly calculating the water vapour concentration of sampled gas based on the hydronium hydrates intensity (of c/s) distribution. However, in order to reduce the systematic difference between the experiment and simulation, we decided to use a dimensionless parameter *H*,

$$H = ln\left(\frac{[H_3O^+] + [H_3O^+.H_2O] + [H_3O^+(H_2O)_2] + \cdots}{[H_3O^+]}\right)$$
$$= ln\left(\frac{i(H_3O^+) + i(H_3O^+.H_2O) + i(H_3O^+(H_2O)_2) + \cdots}{i(H_3O^+)}\right), \quad (21)$$

representing the logarithm of the ratio between all water related reagent and product ions (hydronium and its respective clusters). These values were linearly dependent on the water vapour concentration in the flow-tube.

4. Results

4.1. Complex study of glyoxal ion chemistry

Glyoxal ($C_2H_2O_2$) is the simplest highly reactive dialdehyde. In biological systems, glyoxal is associated with oxidation stress. [116] In the gas phase however, glyoxal may be found as a reaction intermediate in the photo-catalytical reduction of carbon dioxide to methane [117, 118] and also in the earth's atmosphere as a product of the oxidation and photo-oxidation of VOCs (such as toluene, xylene or isoprene) [119-124].

From the stance of chemical ionization, glyoxal represents an analytical challenge as the PA of glyoxal (690 kJ mol^{-1}) estimated by theroretical calculations [125], is simillar to the PA of water (691 kJ mol^{-1}) [126]. Additionaly, neutral glyoxal reacts rapidly with humidity forming a series of oligomers that contribute to the formation of atmospheric aerosol. [116, 127] The ion chemistry of glyoxal with H_3O^+ had been previously studied using SIFT-MS [106, 128], confirming the presence of the proton transfer reaction forming protonated glyoxal. In addition, under increased sample humidity, protonated formaldehyde was also observed. A recent PTR-MS study showed interesting behavior [129] (in contrast to flow tube studies) where the concentration of protonated formaldehyde was very intensive at low humidity, decreasing for higher water vapor concentrations. As none of these studies explained this opposite trend in formation of protonated fornaldehyde, we decided to study this behaviour.

Our study is separated into two parts. Firstly, we investigated glyoxal ion chemistry in the SIFT-MS under variable humidity. This work has already been published and details are in [130]. Secondly, we studied glyoxal's ion chemistry in the presence of an electric field using a PTR-MS as well as a SIFDT-MS instrument. This study has not yet been published, although all details on this work are also available in the form of manuscript, in Attachment A.3 of the thesis.

To summarize, the ion chemistry (for reagent ions in the Profile 3 SIFT-MS: H_3O^+, NO^+ and O_2^+) was investigated, although only H_3O^+ showed a significant change when the water vapour concentration was varied. The high reactivity of neutral glyoxal molecules with water did not allow us to change the humidity of the sample directly.

Instead, we needed to humidify helium carrier gas. Finally, to support study of glyoxal ion chemistry, we also studied the ion chemistry of formaldehyde.

The results confirmed the formation of the protonated glyoxal as the main product ion, as a result of proton transfer from H_3O^+ to glyoxal. An increase in the water concentration leads to the formation of the protonated glyoxal primary hydrate via an association reaction. The protonated glyoxal (primary) hydrate is stable until presented with additional water molecules, resulting in several reaction channels:

$$C_2H_3O_2^+.H_2O + H_2O \leftrightarrow H_3O^+.H_2O + C_2H_2O_2, \quad (22)$$

$$\rightarrow CH_2OH^+ + HCOOH + H_2O, \quad (23)$$

$$C_2H_3O_2^+.H_2O + H_2O + He \rightarrow C_2H_3O_2^+(H_2O)_2 + He. \quad (24)$$

Protonated formaldehyde is formed via the secondary reaction of protonated glyoxal with water (Eq. 23). This assumption was also confirmed by the KIMI simulation, complementing our experimental study.

Additionally, the protonated formaldehyde reacts via a three-body association reaction with water molecules at high system humidity, forming the protonated formaldehyde hydrate. This reaction is of high significance, as the protonated formaldehyde hydrate has the ability to further react with water molecules via a ligand switching reaction into hydronium hydrate:

$$CH_2OH^+ + H_2O + He \rightarrow CH_2OH^+.H_2O + He, \quad (25)$$

$$CH_2OH^+.H_2O + H_2O \rightarrow H_3O^+.H_2O + CH_2O. \quad (26)$$

Reaction 71 is endothermic and relatively slow (5.3×10^{-10} cm^3s^{-1} [131]), however the high number density of water molecules in a humid (up to 3×10^{13} cm^{-3}) reaction equilibrium shifts the system to the production of hydronium hydrate ($H_3O^+.H_2O$). The consequence of this process is a reduction of product ions, characteristic for the detection of glyoxal (when the sample humidity increases).

In conclusion, we clarified that the formation of protonated formaldehyde is caused by the secondary reaction of protonated glyoxal with water vapour. The relative fraction of protonated formaldehyde thus increases with sample humidity. The situation however changes in the presence of an electric field.

Note that the glyoxal ion chemistry was studied using two instruments: the PTR-MS and SIFDT-MS. Important differences in these two methods are found in the type of

buffer gas used in these experiments. While the PTR-MS experiments were carried out in N_2, He was used in SIFDT-MS study. This is significant, as the ion mobility differs between the two buffer gases. The ion mobility determined by the SIFDT instrument is also used in the KIMI simulation and therefore the simulation is unsuitable to be compared to empirical PTR-MS results.

The ion chemistry in both experiments at low *E/N* (where the kinetic energy of ions is close to the thermal energy) follows the reaction pathway found in the SIFT-MS (where protonated formaldehyde is formed via the secondary reaction of protonated glyoxal with water vapour). At high *E/N*, protonated formaldehyde is also formed, although via CID reactions:

$$H_3O^+ + C_2H_2O_2 \rightarrow CH_2OH^+ + HCOOH, \quad (27)$$

$$C_2H_3O_2^+ + BG \rightarrow CH_2OH^+ + CO + BG, \quad (28)$$

where BG represents the respective N_2 and He buffer gases. The calculation of reaction energies in He shows reaction 27 to be more energetic (KE_{CM} = 0.6 eV at *E/N* 50 Td for Eq. 27; KE_{CM} = 0.08 eV at *E/N* 50 Td for Eq. 73). Nevertheless, reaction 28 also contributes to the formation of protonated formaldehyde. Further theoretical calculations are needed to evaluate the energetics and reaction mechanisms for these two processes.

Using the SIFDT-MS experimental results, supplemented by the numerical simulations of the ion chemistry, we were also able to identify the reactions responsible for the decreasing abundance of protonated formaldehyde at increasing sample humidity. Firstly, the humidity decreases the mobility of the primary H_3O^+ reagent ions, resulting in a decrease in reaction energy (in Eq. 27). This leads to a reduction in the formation of protonated formaldehyde. By increasing the water vapour concentration in the drift tube (from dry up to 6.4×10^{13} cm^{-3} water molecules), we observed a 10% reduction in the reaction energy. However, the numerical simulation of the ion chemistry showed that this reduction of reaction energy is not highly significant. What is more significant is the reverse proton transfer reaction of the primary and secondary product ions with water molecules back to the hydronium ion:

$$C_2H_3O_2^+ + H_2O \rightarrow H_3O^+ + C_2H_2O_2, \quad (29)$$

$$CH_2OH^+ + H_2O \rightarrow H_3O^+ + CH_2O. \quad (30)$$

Individual injection of product ions into the humidified drift tube showed that both protonated glyoxal and protonated formaldehyde produce hydronium according to the Arrhenius function. The PA difference between glyoxal and water is almost 0 (based on a theoretical estimation) while the PA differrence between water and formaldehyde is 0.23 eV. [125, 126] This may suggest that reaction 29 proceeds faster compared to reaction 30. The determined ion mobility of protonated formaldehyde is however larger compared to the ion mobility of the protonated glyoxal product ion and consiquenly the relative KE_{CM}. For increasing *E/N*, the KE_{CM} for Eq. 30 increaseses faster compared to Eq. 29 and tehrefore the reaction rate for Eq. 30 will eventually overtake the reaction rate of Eq. 29. This equlilibrium change is also seenin the ion chemistry of glyoxal at high *E/N*. An increase of humidity causes protonated formaldehyde to convert into hydronium faster compared to protonated glyoxal. This in turn reduces the concentraion of protonated formaldehyde, relative to protonated glyoxal. Numerical simulations of the proposed reaction mechanisms confirm this behaviour.

It is important to note that the aim of KIMI simulation was not to fully interpolate experimental data, but to explain the chemical mechanisms leading to the experimentally observed data. The simulation uses several approximations covering various reaction parameters. Further theoretical and experimental work is however required (especially for the purposes of fully simulating PTR-MS data).

4.2. Ion chemistry of phthalates studied by SIFT-MS

Phthalates (esters of phthalic acid) are used as plasticizers in the production of plastics. Their negative health effects on human genitalia have however been reported [132, 133]. To date, phthalates have been characterized as endocrine disruptors making this species of chemicals hazardous for pregnant women and children under the age of 3 years. Several of the most dangerous phthalate compounds are under EU regulations [134] or are tracked by the European Chemical Agency (*EHCA*) [135]. For the exception of children's toys, the regulations surrounding phthalates imposed by the EHCA do not cover any other daily plastic products (i.e. plastic containers [136], cosmetics [137], toothbrushes [138] and more). Such plastic products which can be bought in Europe are predominantly manufactured in countries such as China and India

where the EHCA (or any other regulatory body) does not prohibit the regulation of phthalate contamination within these plastics. Plastic products imported into the EU should therefore be more controlled.

Several analytical techniques are used for the detection of phthalates; mainly liquid or gas chromatography coupled to mass spectrometry (GC-MS / LC-MS) [139] primarily using electron ionization at 70 eV. The primary product of dissociative ionization which is shown in the mass spectrum is the protonated phthalate anhydride (*m/z* 149), which characteristic for most phthalates [126]. The presence of a phthalate species may be confirmed by the detection of the phthalate anhydride ion; however, mass spectrometry measurements possess poor selectivity (phthalate species dependant). Using chemical ionization, individual phthalate species may be identified. [140] Ion mobility spectrometry (IMS) is a suitable SCI technique for the detection of phthalates. SCIMS techniques may potentially be used for real time analysis and for the accurate detection of phthalate contamination in plastics. The ability to achieve this has already been demonstrated by Michalczuk et al. [141]. As IMS operates near atmospheric pressure, analyte molecules react mainly with hydronium clusters $H_3O^+(H_2O)_n$.

To evaluate the ability of these methods in detecting phthalate species using IMS, one first needs to understand the ion chemistry. To aid us in this understanding, we present a study of several simple phthalates: dimethyl phthalate (DMP), dimethyl isophthalate (DMIP), dimethyl terephthalate (DMTP), diethyl phthalate (DEP), dipropyl phthalate (DPrP) and dibutyl phthalate (DBP); from SIFT-MS experiments. The study focuses on phthalate ion chemistry when these molecules interact with $H_3O^+(H_2O)_n$ primary ions. The respective isomerization effects are also discussed, which compliments the previous work by Michalczuk et al. [141].

A full description of our experiments, results and the corresponding discussion are presented in [142] (as this study has already been published). In this work, the phthalate ion chemistry was studied by using H_3O^+, NO^+ and O_2^+ reagent ions under variable system humidification. Depending on the reagent ion used, the type of interaction occurring between the sample molecule and the bombarding ion may either (primarily) be a proton transfer reaction (H_3O^+)**;** a charge transfer process (O_2^+); or a charge transfer or association process (NO^+).

Previously recorded IMS/MS studies show that the location of ester groups on a benzene core significantly changes the ability for clustering (hydration) of phthalate isomers to hydrate. The 1,2 position (DMP) of an ester group does not provide an accessible angle for hydrogen bonding to occur and does not allow for stable hydrate formation. The presence of phthalate esters on carbons 1 and 3 (DMIP) does however allow for the effective association of two water molecules. The [fully open] 1,4 isomer of phthalate esters (DMTP) effectively binds only one water molecule. These observations were also confirmed in our SIFT-MS studies. The effect of humidity on the ion chemistry is based on two main aspects. The first is the interaction of reagent ion with water molecules, forming water clusters of reagent ions which goes on to affect the ion chemistry. The second aspect is the presence of secondary reactions between products of primary reactions and water molecules. The effect of humidity on the ion chemistry was mainly studied for H_3O^+ reagent ions, where it has the most significant impact.

In our investigation we observed differences between the IMS and SIFT-MS ion chemistry, namely the formation of $(M\text{-}OR)^+$ (characteristic for CI and EI ionization not observed in IMS, presumably, due to the higher pressure). The effect of isomerization on the formation of phthalate hydrates for DMP, DMIP and DMTP has been explained using a computational DFT theoretical approach, showing that the energetic difference between individual states of hydration for *ortho* isomers is very small. Therefore, at a high number density of water molecules, the reaction equilibrium moves in favour of the dominant formation of protonated DMP. The remaining isomers have their energetic minima for the hydration process lower and therefore the formation of protonated hydrates is possible. Finally, we used KIMI simulations to clarify the reaction channels leading to the formation of protonated phthalate hydrates. We confirmed that the hydrates are formed through sequential association reactions of the protonated phthalate entity with water molecule, rather than via ligand switching reaction between hydronium hydrates and neutral phthalates. The presented work helps one to understand the ion chemistry of phthalates in SCIMS and reveals the additional possibilities of differentiating phthalate isomers using their secondary reactivity in the presence of water vapour.

4.3 Study of secondary ligand switching reactions of protonated acetic acid hydrates with acetone

Ligand switching reactions are important ionization mechanisms at atmospheric or near-atmospheric pressure and covers the IMS and SESI analytical techniques. The presence of such processes is crucial for analytical applications. If an analysed sample contains several neutral reactants, the primary ionization reactions between the reagent ions and neutral reactants may also be supplemented by secondary reactions (between the product ions of primary ionization channels and the remaining reactant neutrals). For example, a polar organic molecule, A, reacting via ligand switching with hydronium hydrates

$$H_3O^+(H_2O)_n + A \rightarrow AH^+(H_2O)_n + H_2O \quad (31)$$

can additionally react with a second polar molecule, M, also via ligand switching, replacing A or forming a proton-bound mixed dimer:

$$AH^+(H_2O)_n + M \rightarrow MH^+(H_2O)_n + A \quad (32a)$$

$$\rightarrow AH^+(M)(H_2O)_{n-1} + H_2O. \quad (32b)$$

If the molecule, M, is abundant in the system, secondary ligand switching processes may lead to the replacement of A, forming a symmetrical dimer:

$$AH^+(M)(H_2O)_n + M \rightarrow MH^+M + A + nH_2O. \quad (33)$$

This processes clearly complicates analytical methods, decreasing selectivity and sensitivity of particular components in a sample.

Such an effect needs to be considered in SESI-MS studies of exhaled breath. Studies have shown that the concentration of acetic acid in exhaled breath is typically a hundred times lower than the concentration of acetone. [37, 143, 144] In the present work, we studied such effects, specifically looking at the secondary ligand switching reactions between acetic acid hydrates and acetone vapours. The study was carried out using the new generation of SIFDT-MS instrument, (developed at the J. Heyrovsky institute by Dr. Spesyvyi) equipped with an ion source capable of generating protonated hydrates of acetic acid (see Fig 5). In the experiment, hydrated and protonated acetic acid clusters, $CH_3COOH.H^+(H2O)_2$ were generated in the ion source and filtered via an injection filter. These ions were subsequently fragmented via a CID at the entrance of the drift tube, into the hydrated protonated acetic acid entity,

$CH_3COOH.H^+.H_2O$, by using a high kinetic transmission energy for $CH_3COOH.H^+(H2O)_2$ ions in the injection quadrupole. The drift tube operated at a low *E/N* = 14.2 Td was used to study the reaction of hydrated protonated acetic acid with acetone in the presence of a helium carrier gas (at a pressure of 1.9 mbar and temperature of 293 K). This complex experimental study was supplemented by the theoretical DFT calculations of individual protonated hydrates, as well as KIMI simulations of a proposed set of reactions.

This work has already been published and all details may be found in [31]. This case study demonstrates the possibility of instigating study ligand switching reactions in the SIFDT-MS. We also characterised specific ligand switching reactions between protonated acetic acid hydrates and acetone, relevant for breath analysis.

4.4 Real time detection of Arsene and Selene hydrides by SIFT-MS

SCIMS techniques are mainly used for real-time trace analysis of VOCs. However, SCIMS is not limited to only organic analytes, but may also be used for any compound reacting rapidly with one of the primary reagent ions (H_3O^+, NO^+ and O_2^+). In the present study, we investigated the possibility of being able to analyse the inorganic volatile species selenium hydride (SeH_2), arsenic hydride (AsH_3), monomethylarsane (CH_3AsH_2) and dimethylarsane ($(CH_3)_2AsH$). These are all relevant for the detection of Arsenic and Selenic elements in atomizers.

Atomization is a popular method for the trace element analysis of several elements (As, Se, Sb, Sn, …) and is conducted via the generation of volatile hydrides. [145] These are produced from an analyte in the liquid phase, using the reaction between tetrahydridoborate(-1) (TBH) and an acid. This achieves almost 100% conversion (in some cases). During the reaction, the analyte is released into the gaseous phase in form of a volatile hydride where it may be detected by various techniques. It is assumed that the relation between the active hydride species (for example MAs^V) and the volatile hydrides (for example CH_3AsH_2) is explicit (i.e. the specific hydride active species produce specific volatile hydrides). This argument was however questioned by Talmi and Bostick (1975), who suggested that the reaction may be pH dependent. [146]

Generated volatile hydrides are mainly detected by atomic absorption spectrometry. Consequently, volatile hydrides are often decomposed after their generation into atomic species using a quartz tube atomizer, heated up to 900 °C. [147, 148]. Besides standard atomization (decomposing volatiles by heat), plasma dielectric barrier discharge (DBD) atomizers may also be used [149]. In the present study, the SIFT-MS was used to analyse the formation and atomization of selected hydrides in a DBD atomizer. This study was conducted in cooperation with the Institute of Analytical Chemistry of the Czech Academy of Science.

Aside to the volatile hydrides generated from a liquid solution, several other molecules are present in the sample as well: hydrogen gas as a by-product of hydride generation; argon as a carrier gas; water vapour from the sample solution and traces of oxygen penetrating into the generator gas lines. To reduce sample humidity for arsene hydrides, NaOH pellets were introduced into the sample gas line. For selenium hydrides, dryers however cannot be applied, as selenium hydrides, compared to arsenic hydrides, are affected by the presence of a drying agent. The presence of hydrogen gas in the atomizer is crucial as it reacts together with traces of oxygen within the plasma, to produce water. Water consequently influences the property of the DBD discharge, affecting the atomization.

In our study, we first confirmed the formation of the protonated hydrides of all the studied species, in our SIFT-MS. Secondly, we analysed the concentration of the protonated hydrides in the DBD atomizer, together with the formation of secondary products (predominantly H_2O). Finally, we introduced an excess of oxygen gas into the sample to characterize the effect of H_2O on the atomization process in the DBD. As the study has also already been published, all details surrounding this work may be found in [150].

The present study shows a new application of SCIMS, which goes beyond the detection and analysis of VOCs. We have shown that SIFT-MS, as well as all other SCIMS techniques, may be implemented in the analytical applications of inorganic chemistry. This may either be conducted by direct (or indirect) analysis of inorganic volatile compounds (helping us to understand established analytical procedures, such as atomization).

Conclusion

In conclusion, this thesis discusses the ion chemistry processes used for trace gas analysis carried out by CI-MS techniques, operating in the mbar pressure range. The focus was to understand the limitations of SCIMS techniques; mainly on the aspects of reduced selectivity and sensitivity. Besides many positives (such as high sensitivity, a large dynamic range and a real-time response for most of the VOCs detected), the SCIMS techniques demonstrate limited ability to conduct selective analysis of isomeric molecules. Additionally, water vapour present in the reaction chamber of the instruments (introduced by sample humidity) may reduce sensitivity and selectivity of the analytes, via the secondary reactions of water molecules with ions.

The main objectives of the thesis were to analyse the limitations of these techniques which reduced the sensitivity and selectivity of the SCIMS methods, via the study of complex ion chemistry. This work predominantly focused on secondary reactions with water. Additionally, we aimed to provide a mathematical description of the associated primary and secondary reactions which made it capable to predict the behaviour of the relative ion signals. The mathematical description will be supplemented by an experimental study of complex ion-molecular reactions relevant to typical SCIMS applications (such as breath analysis, environmental science etc.). Finally, we aimed to investigate the new possible applications for SCIMS analysis.

We first presented a unique combination of a fast GC pre-separation unit, coupled to a SIFT-MS experiment. This set-up was developed to try and improve the analytical selectivity of monoterpenes; common isomers in investigated in atmospheric chemistry when studying the formation of secondary organic aerosol; and air quality. In this work, we combined a fast-chromatographic separation technique with the SIFT-MS. As a result, we identified individual isomers of the monoterpene family in under 45 s, using an MXT-1 metallic column in association with the calculation for the ion ratio of the two product ion pairs, generated by H_3O^+ (*m/z* 137 / *m/z* 81) and NO^+ (*m/z* 136 / *m/z* 93). The relative intensities of the fragment ions were shown to be characteristic for the individual monoterpenes. However, we also found that the sample flow rate from the GC column (< 4 sccm) is not sufficient to achieve a sub-ppbv detection limit, which is commonly achieved by fast GC PTR-MS. Interestingly, we also noticed that water vapour has a retention time which is much lower compared

to the VOCs detected the samples that we ran. Therefore, fast GC may potentially be used to separate VOCs from sample humidity. This may therefore be a welcomed benefit to the field as water vapour often influences the ion chemistry within these CIMS techniques. In addition, a high humidity within the instrument reduces the selectivity and sensitivity of the methods.

The experimental and mathematical studies conducted of the influence of water vapour on the ion chemistry of the discussed techniques makes-up the main body of this work. We first developed a numerical simulation for the computational investigation of ion-molecule reactions (KIMI) and carried out two sets of experiments. In these experiments we focused on understanding the secondary reactions of product ions with water (the study of the ion chemistry of glyoxal and phthalates).

KIMI is a simple numerical simulator capable of mathematically describing complex reaction systems. The simulator solves a set of differential equations based on a proposed reaction system along the axis of the reactor using the classical Runge-Kutta algorithm. Therefore, KIMI is capable of simulating the ion chemistry which occurs within the SIFT-MS, PTR-MS as well as the SIFDT-MS instruments. To demonstrate its functionality, KIMI was first tested on several simple and well understood reaction systems (i.e. acetone and alcohols), where we observed changes in the product ion distribution. On successfully simulating this chemistry, we later used our KIMI program to investigate more complex reaction systems.

The glyoxal study was divided into two sections. The first part describes the ion chemistry and the associated secondary reactions with water vapour in a flow tube (where we identified the water induced generation of protonated formaldehyde). The second section describes a similar situation for the drift tube, where protonated formaldehyde is also generated; via CID. The aim of the of the drift tube study was to explain the changes in the relative ratios of the main product ions to the protonated formaldehyde and protonated glyoxal ions. Using several experimental techniques together with KIMI, we identified the secondary reactions responsible for the observed changes (primarily induced via secondary reverse proton transfer reactions).

In the study of phthalates, our objective was to describe the ion chemistry of selected phthalates with H_3O^+, NO^+ and O_2^+ reagent ions (as well as the secondary reactions of selected protonated phthalates, with water vapour). The list of selected phthalates

included the DMP, DMIP and DMTP isomers. These were chosen to study the effect of varying the position and length of the substituents around the benzene ring on the ion chemistry. The length of the phthalate substituent prominently affects the ion chemistry of charge transfer reactions via the opening of a new rearrangement channel leading to the formation of $(M-(R-2H))^+$ products. The secondary reactions (with water molecules) were also studied for the protonated phthalate molecules. We have demonstrated that protonated phthalates in the *ortho* position do not form hydrides. For the isomers with *meta* and *para* geometries, however, phthalates form hydrides very effectively. For the DMTP isomer, we detected the association of one H_2O molecule to the analyte ion. For DMIP, we detected the clustering of a second H_2O molecule. The hydration does not continue to form any larger clusters, as a strong potential minimum exist only for the specific DMTP and DMIP structures. Finally, we used KIMI to confirm that the protonated phthalate hydrates in the flow tube were formed via the association of water molecules on the protonated phthalate, rather than via ligand switching of the H_2O molecules with hydrated hydronium.

The initial product ions may however (additional to analyte) also react with other abundant neutral molecules in secondary reactions. Subsequently, we studied such reactions between protonated acetic acid hydrates and acetone. This reaction system is interesting as both acetic acid and acetone are abundant and analytically important components in breath analysis. In breath analysis carried out by SESI-MS or IMS techniques in the near-to-atmospheric pressure region of conditions, ion hydrates are formed frequently. As we have shown, hydrates of protonated acetic acid (reflecting the concentration of acetic acid in the sample) undergo secondary ligand switching reactions with acetone. This process leads to the fast formation of the asymmetric proton-bounded dimer $(CH_3COCH_3)H^+(CH_3COOH)$ and ultimately the production of the strongly bound protonated-acetone dimer. This reaction sequence was also simulated using KIMI. This study clearly demonstrates that the presence of highly abundant polar compounds in SESI-MS and IMS may negatively affect the accuracy of quantification of other analytes at low concentrations.

In summary, the presence of secondary reactions complicates the identification and quantification of absolute concentrations of species in SCIMS techniques. The most abundant cause of secondary reactions are water molecules, resulting from sample humidity. Water molecules react with product ions via several secondary reaction

channels. In the present work, we identified three secondary reaction channels which were seen to be the most detrimental to accurate analysis of species when using SCIMS techniques:

1. Three-body association reactions forming ion hydrates of both reagent and product ions.

2. Reverse proton transfer reactions between product ions (or their hydrates) and water molecules (Eq. 20).

3. Reaction channels between product ions and water molecules, producing new and unexpected ions.

The last point reflects the most interesting part of the ion chemistry. An example of point 3 is the formation of protonated formaldehyde from protonated glyoxal via a series of water assisted reactions; or secondary formation of protonated phthalate while using NO^+ reagent ions, via the reaction:

$$M.NO^+ + H_2O \rightarrow MH^+ + HONO. \quad (34)$$

Additionally, secondary reactions are not only induced by water vapour, but also by other molecules present at sufficiently high concentrations in the reaction chamber. (see study of secondary ligand switching reactions of protonated acetic acid hydrates with acetone, section 4.3).

The effect of the secondary reactions may be minor, but also significant, depending on the analytical situation. So far, we are able to identify three different approaches to reduce the impact of secondary reactions on analysis. The first approach is to carefully increase the effective temperature of the gases in the flow tube (as for example in PTR-MS or SIFDT-MS), as to reduce the formation of ion hydrates. This may however induce both a reverse proton transfer reaction as well as a new reaction channel (as we observed in the glyoxal study). The second approach is to remove the humidity from the sample (either via filters or via pre-separation using the fast GC technique we developed). This however reduces the speed of SCIMS as well as limits its sensitivity. The last approach is an understanding the water-based ion chemistry. This however requires a careful and systematic; theoretical and experimental study of complex reaction systems.

In the final study we pioneered the possibility of using SCIMS for the analysis of inorganic volatile hydrides, produced during atomization. The process of atomization is used to quantify the absolute concentrations of inorganic species of germanium, arsenic, tin etc., primarily in solid samples. The inorganic species are in controlled environments; chemically converted into hydrides. Volatile hydrides are then atomized using a quartz tube or discharge-based atomizers; and are detected via atomic absorption spectrometry. In this study, we investigated the possibility of detecting selected hydrides of selenium and arsenic using SIFT-MS which has in-turn helped us to understand the process of atomisation in dielectric barrier discharge (DBD) under various conditions, much better. The focus of this study was to analyse non-atomised hydrides and subsequently evaluate the effectivity of the atomization process. We have shown that the hydrides are not always atomised; but are often decomposed in the DBD. Additionally, atomization is affected by humidity which is delivered to the atomizer from the sample or is formed in the atomizer via the by-reaction of residual hydrogen and oxygen. The possibility of SCIMS to detect non-atomised hydrides as well as humidity levels is of high interest.

The presented work fulfils the defined objectives of the thesis, as well as the aims of the IMPACT project. The obtained results reported in this thesis have been frequently presented at conferences on the national and international stage. So far, our results have led to the production of 5 high-impact publications; and more publications based on these works are expected to be published soon. The KIMI simulator is still under development but may already be used to assist with ion-molecule interaction research. We believe that the knowledge gained from this work will help to improve the application of current as well as future SCIMS technologies.

List of publications

Lacko M, Wang N, Sovová K, Pásztor P, Španěl P.
Addition of fast gas chromatography to selected ion flow tube mass spectrometry for analysis of individual monoterpenes in mixtures.
Atmospheric Measurement Techniques. 2019. 12(9): 4965-82.

Lacko M, Piel F, Mauracher A, Španěl P.
Chemical ionization of glyoxal and formaldehyde with H_3O^+ ions using SIFT-MS under variable system humidity.
Physical Chemistry Chemical Physics. 2020. 22(18): 10170-10178

Lacko M, Michalczuk B, Matejčík Š, Španěl P.
Ion chemistry of phthalates in selected ion flow tube mass spectrometry: isomeric effects and secondary reactions with water vapour.
Physical Chemistry Chemical Physics. 2020. 22(28): 16345-52.

Spesyvyi A, **Lacko M**, Dryahina K, Smith D, Španěl P.
Ligand Switching Ion Chemistry: An SIFDT Case Study of the Primary and Secondary Reactions of Protonated Acetic Acid Hydrates with Acetone.
Journal of the American Society for Mass Spectrometry. 2021. 32(8): 2251-60.

Kratzer J, **Lacko M**, Dryahina K, Matoušek T, Španěl P, Dědina J.
Atomization of As and Se volatile species in a dielectric barrier discharge atomizer after hydride generation: Fate of analyte studied by selected ion flow tube mass spectrometry.
Analytica chimica acta. 2022. 1190: 339256.

Bibliography

1. Langevin, M. *Une formule fondamentale de théorie cinétique*. in *Annales de chimie et de physique, Series*. 1905.
2. Moran, T.F. and W.H. Hamill, *Cross Sections of Ion–Permanent‐Dipole Reactions by Mass Spectrometry.* The Journal of Chemical Physics, 1963. **39**(6): p. 1413-1422.
3. Su, T. and M.T. Bowers, *Ion-polar molecule collisions: the effect of ion size on ion-polar molecule rate constants; the parameterization of the average-dipole-orientation theory.* International Journal of Mass Spectrometry and Ion Physics, 1973. **12**(4): p. 347-356.
4. Bass, L., et al., *Ion-polar molecule collisions. A modification of the average dipole orientation theory: The cos θ model.* Chemical Physics Letters, 1975. **34**(1): p. 119-122.
5. Su, T. and M.T. Bowers, *Parameterization of the average dipole orientation theory: temperature dependence.* International Journal of Mass Spectrometry and ion processes, 1975. **17**: p. 211-212.
6. Chesnavich, W.J., T. Su, and M.T. Bowers, *Collisions in a noncentral field: a variational and trajectory investigation of ion–dipole capture.* The Journal of Chemical Physics, 1980. **72**(4): p. 2641-2655.
7. Zhao, J. and R. Zhang, *Proton transfer reaction rate constants between hydronium ion (H 3 O+) and volatile organic compounds.* Atmospheric Environment, 2004. **38**: p. 2177-2185.
8. Bohme, D.K., G.-I. Mackay, and H. Schiff, *Determination of proton affinities from the kinetics of proton transfer reactions. VII. The proton affinities of O2, H2, Kr, O, N2, Xe, CO2, CH4, N2O, and CO.* The Journal of Chemical Physics, 1980. **73**(10): p. 4976-4986.
9. Field, F. and F. Lampe, *Reactions of gaseous ions. VI. Hydride ion transfer reactions.* Journal of the American Chemical Society, 1958. **80**(21): p. 5587-5592.
10. Spanel, P. and D. Smith, *SIFT studies of the reactions of H3O+, NO+ and O2+ with a series of alcohols.* International journal of mass spectrometry and ion processes, 1997. **167**: p. 375-388.
11. Španěl, P., T. Wang, and D. Smith, *A selected ion flow tube, SIFT, study of the reactions of H3O+, NO+ and O2+ ions with a series of diols.* International Journal of Mass Spectrometry, 2002. **218**(3): p. 227-236.
12. Ŝpaněl, P. and D. Smith, *SIFT studies of the reactions of H3O+, NO+ and O+ 2 with a series of volatile carboxylic acids and esters.* International journal of mass spectrometry and ion processes, 1998. **172**(1-2): p. 137-147.
13. Lau, Y., S. Ikuta, and P. Kebarle, *Thermodynamics and kinetics of the gas-phase reactions H3O+ (H2O) n-1+ water= H3O+ (H2O) n.* Journal of the American Chemical Society, 1982. **104**: p. 1462-1469.
14. Wannier, G.H., *Motion of gaseous ions in strong electric fields.* The Bell System Technical Journal, 1953. **32**(1): p. 170-254.
15. Albritton, D., et al., *Effects of ion speed distributions in flow‐drift tube studies of ion‐neutral reactions.* The Journal of Chemical Physics, 1977. **66**(2): p. 410-421.

16. Viehland, L.A. and E. Mason, *Statistical–mechanical theory of gaseous ion–molecule reactions in an electrostatic field.* The Journal of Chemical Physics, 1977. **66**(2): p. 422-434.
17. Su, T., *Parametrization of kinetic energy dependences of ion–polar molecule collision rate constants by trajectory calculations.* The Journal of chemical physics, 1994. **100**(6): p. 4703-4703.
18. Kebarle, P., *Ion thermochemistry and solvation from gas phase ion equilibria.* Annual Review of Physical Chemistry, 1977. **28**(1): p. 445-476.
19. Pierce, R.C. and R.F. Porter, *Low-temperature chemical ionization mass spectrometry of methane-hydrogen mixtures.* The Journal of Physical Chemistry, 1974. **78**(2): p. 93-97.
20. Abramson, F.P. and J.H. Futrell, *Ion—Molecule Reactions of Methane.* The Journal of Chemical Physics, 1966. **45**(6): p. 1925-1931.
21. Durup‐Ferguson, M., et al., *Enhancement of charge‐transfer reaction rate constants by vibrational excitation at kinetic energies below 1 eV.* The Journal of Chemical Physics, 1983. **79**(1): p. 265-272.
22. Viggiano, A. and R.A. Morris, *Rotational and Vibrational Energy Effects on Ion− Molecule Reactivity as Studied by the VT-SIFDT Technique.* The Journal of Physical Chemistry, 1996. **100**(50): p. 19227-19240.
23. Glosik, J., et al., *Energy dependencies of fast reactions of positive ions X+ with HCl from near thermal to≈ 2 eV center‐of‐mass collision energy (X+= H+, H2+, H3+, N+, N2+, Ar+, C+, CH+, CH2+, CH3+, CH4+, CH5+).* The Journal of chemical physics, 1993. **98**(9): p. 6995-7003.
24. Spesyvyi, A., D. Smith, and P. Španěl, *Selected ion flow-drift tube mass spectrometry: quantification of volatile compounds in air and breath.* Analytical chemistry, 2015. **87**(24): p. 12151-12160.
25. Adams, N. and D. Smith, *The selected ion flow tube (SIFT); a technique for studying ion-neutral reactions.* International Journal of Mass Spectrometry and Ion Physics, 1976. **21**(3-4): p. 349-359.
26. Smith, D. and N. Adams, *The selected ion flow tube (SIFT): studies of ion-neutral reactions.* Advances in atomic and molecular physics, 1988. **24**: p. 1-49.
27. Smith, D. and P. Španěl, *Selected ion flow tube mass spectrometry (SIFT‐MS) for on‐line trace gas analysis.* Mass spectrometry reviews, 2005. **24**(5): p. 661-700.
28. Lindinger, W., A. Hansel, and A. Jordan, *On-line monitoring of volatile organic compounds at pptv levels by means of proton-transfer-reaction mass spectrometry (PTR-MS) medical applications, food control and environmental research.* International Journal of Mass Spectrometry and Ion Processes, 1998. **173**(3): p. 191-241.
29. Keck, L., U. Oeh, and C. Hoeschen, *Corrected equation for the concentrations in the drift tube of a proton transfer reaction-mass spectrometer (PTR-MS).* International Journal of Mass Spectrometry, 2007. **264**(1): p. 92-95.
30. Spesyvyi, A. and P. Španěl, *Determination of residence times of ions in a resistive glass selected ion flow‐drift tube using the Hadamard transformation.* Rapid Communications in Mass Spectrometry, 2015. **29**(17): p. 1563-1570.
31. Spesyvyi, A., et al., *Ligand Switching Ion Chemistry: An SIFDT Case Study of the Primary and Secondary Reactions of Protonated Acetic Acid Hydrates*

with Acetone. Journal of the American Society for Mass Spectrometry, 2021. **32**(8): p. 2251-2260.
32. Miekisch, W., J.K. Schubert, and G.F. Noeldge-Schomburg, *Diagnostic potential of breath analysis—focus on volatile organic compounds.* Clinica chimica acta, 2004. **347**(1-2): p. 25-39.
33. Španěl, P. and D. Smith, *Progress in SIFT‐MS: Breath analysis and other applications.* Mass spectrometry reviews, 2011. **30**(2): p. 236-267.
34. Bruderer, T., et al., *On-line analysis of exhaled breath: focus review.* Chemical reviews, 2019. **119**(19): p. 10803-10828.
35. Španěl, P. and D. Smith, *Quantification of volatile metabolites in exhaled breath by selected ion flow tube mass spectrometry, SIFT-MS.* Clinical Mass Spectrometry, 2020. **16**: p. 18-24.
36. Storer, M., et al., *Measurement of breath acetone concentrations by selected ion flow tube mass spectrometry in type 2 diabetes.* Journal of Breath Research, 2011. **5**(4): p. 046011.
37. Dryahina, K., et al., *Exhaled breath concentrations of acetic acid vapour in gastro-esophageal reflux disease.* Journal of breath research, 2014. **8**(3): p. 037109.
38. Ratiu, I.-A., et al., *Mass spectrometric techniques for the analysis of volatile organic compounds emitted from bacteria.* Bioanalysis, 2017. **9**(14): p. 1069-1092.
39. Shestivska, V., et al., *Quantification of methyl thiocyanate in the headspace of Pseudomonas aeruginosa cultures and in the breath of cystic fibrosis patients by selected ion flow tube mass spectrometry.* Rapid Communications in Mass Spectrometry, 2011. **25**(17): p. 2459-2467.
40. Shestivska, V., et al., *Variability in the concentrations of volatile metabolites emitted by genotypically different strains of Pseudomonas aeruginosa.* Journal of Applied Microbiology, 2012. **113**(3): p. 701-713.
41. Gilchrist, F.J., et al., *Hydrogen cyanide concentrations in the breath of adult cystic fibrosis patients with and without Pseudomonas aeruginosa infection.* Journal of breath research, 2013. **7**(2): p. 026010.
42. Smith, D., et al., *Breath concentration of acetic acid vapour is elevated in patients with cystic fibrosis.* Journal of breath research, 2016. **10**(2): p. 021002.
43. Davies, S.J., P. Španěl, and D. Smith, *Breath analysis of ammonia, volatile organic compounds and deuterated water vapor in chronic kidney disease and during dialysis.* Bioanalysis, 2014. **6**(6): p. 843-857.
44. Kohl, I., et al., *First observation of a potential non-invasive breath gas biomarker for kidney function.* Journal of breath research, 2013. **7**(1): p. 017110.
45. Eng, K., et al., *Analysis of breath volatile organic compounds in children with chronic liver disease compared to healthy controls.* Journal of breath research, 2015. **9**(2): p. 026002.
46. Lembo, V., et al., *Rapid" breath-print" of liver cirrhosis by Proton Transfer Reaction Time of Flight Mass Spectrometry.* 2013.
47. Smolinska, A., et al., *Profiling of volatile organic compounds in exhaled breath as a strategy to find early predictive signatures of asthma in children.* PloS one, 2014. **9**(4): p. e95668.

48. Kharitonov, S.A. and P.J. Barnes, *Exhaled markers of pulmonary disease.* American journal of respiratory and critical care medicine, 2001. **163**(7): p. 1693-1722.
49. Dryahina, K., et al., *Quantification of pentane in exhaled breath, a potential biomarker of bowel disease, using selected ion flow tube mass spectrometry.* Rapid Communications in Mass Spectrometry, 2013. **27**(17): p. 1983-1992.
50. Lechner, M., et al., *Headspace screening of fluid obtained from the gut during colonoscopy and breath analysis by proton transfer reaction-mass spectrometry: A novel approach in the diagnosis of gastro-intestinal diseases.* International Journal of Mass Spectrometry, 2005. **243**(2): p. 151-154.
51. Phillips, M., et al., *Volatile organic compounds in breath as markers of lung cancer: a cross-sectional study.* The Lancet, 1999. **353**(9168): p. 1930-1933.
52. Williams, J., et al., *An atmospheric chemistry interpretation of mass scans obtained from a proton transfer mass spectrometer flown over the tropical rainforest of Surinam.* Journal of Atmospheric Chemistry, 2001. **38**(2): p. 133-166.
53. Crutzen, P., et al., *High spatial and temporal resolution measurements of primary organics and their oxidation products over the tropical forests of Surinam.* Atmospheric Environment, 2000. **34**(8): p. 1161-1165.
54. Warneke, C., et al., *Isoprene and its oxidation products methyl vinyl ketone, methacrolein, and isoprene related peroxides measured online over the tropical rain forest of Surinam in March 1998.* Journal of Atmospheric Chemistry, 2001. **38**(2): p. 167-185.
55. Müller, K., et al., *Biogenic carbonyl compounds within and above a coniferous forest in Germany.* Atmospheric Environment, 2006. **40**: p. 81-91.
56. Rinne, J., et al., *On-line PTR-MS measurements of atmospheric concentrations of volatile organic compounds in a European boreal forest ecosystem.* Boreal environment research, 2005. **10**(5): p. 425-436.
57. Williams, J., et al., *The summertime Boreal forest field measurement intensive (HUMPPA-COPEC-2010): an overview of meteorological and chemical influences.* Atmospheric Chemistry and Physics, 2011. **11**(20): p. 10599-10618.
58. Ammann, C., et al., *Application of PTR-MS for measurements of biogenic VOC in a deciduous forest.* International Journal of Mass Spectrometry, 2004. **239**(2-3): p. 87-101.
59. Fall, R., et al., *Biogenic C5 VOCs: release from leaves after freeze–thaw wounding and occurrence in air at a high mountain observatory.* Atmospheric Environment, 2001. **35**(22): p. 3905-3916.
60. Karl, T., et al., *High concentrations of reactive biogenic VOCs at a high altitude site in late autumn.* Geophysical Research Letters, 2001. **28**(3): p. 507-510.
61. Fares, S., et al., *Biogenic emissions from Citrus species in California.* Atmospheric Environment, 2011. **45**(27): p. 4557-4568.
62. Misztal, P.K., et al., *Large estragole fluxes from oil palms in Borneo.* Atmospheric Chemistry and Physics, 2010. **10**(9): p. 4343-4358.
63. Misztal, P.K., et al., *Direct ecosystem fluxes of volatile organic compounds from oil palms in South-East Asia.* Atmospheric Chemistry and Physics, 2011. **11**(17): p. 8995-9017.

64. Kammer, J., et al. *Effect of agricultural practices on volatile organic compound (VOC) emissions from winter wheat*. in *8 th International PTR-MS Conference 2019*. 2019.
65. Holzinger, R., et al., *Diurnal cycles and seasonal variation of isoprene and its oxidation products in the tropical savanna atmosphere.* Global Biogeochemical Cycles, 2002. **16**(4): p. 22-1-22-13.
66. Bamberger, I., et al., *BVOC fluxes above mountain grassland.* Biogeosciences, 2010. **7**(5): p. 1413-1424.
67. Davison, B., et al., *Cut-induced VOC emissions from agricultural grasslands.* Plant Biology, 2007. **9**(S 01): p. e60-e68.
68. Sovová, K., et al., *Time-integrated thermal desorption for quantitative SIFT-MS analyses of atmospheric monoterpenes.* Analytical and bioanalytical chemistry, 2019. **411**(14): p. 2997-3007.
69. Bsaibes, S., et al., *Monoterpene Chemical Speciation with High Time Resolution Using a FastGC/PTR-MS: Results from the COV3ER Experiment on Quercus ilex.* Atmosphere, 2020. **11**(7): p. 690.
70. Shaw, S.L., et al., *Volatile organic compound emissions from dairy cows and their waste as measured by proton-transfer-reaction mass spectrometry.* Environmental science & technology, 2007. **41**(4): p. 1310-1316.
71. Feilberg, A., et al., *Odorant emissions from intensive pig production measured by online proton-transfer-reaction mass spectrometry.* Environmental Science & Technology, 2010. **44**(15): p. 5894-5900.
72. Hansen, M.J., et al., *Application of proton-transfer-reaction mass spectrometry to the assessment of odorant removal in a biological air cleaner for pig production.* Journal of Agricultural and Food Chemistry, 2012. **60**(10): p. 2599-2606.
73. Sprung, D., et al., *Acetone and acetonitrile in the tropical Indian Ocean boundary layer and free troposphere: Aircraft‐based intercomparison of AP‐CIMS and PTR‐MS measurements.* Journal of Geophysical Research: Atmospheres, 2001. **106**(D22): p. 28511-28527.
74. Sinha, V., et al., *Air-sea fluxes of methanol, acetone, acetaldehyde, isoprene and DMS from a Norwegian fjord following a phytoplankton bloom in a mesocosm experiment.* Atmospheric Chemistry and Physics, 2007. **7**(3): p. 739-755.
75. Williams, J., et al., *Measurements of organic species in air and seawater from the tropical Atlantic.* Geophysical research letters, 2004. **31**(23).
76. Wang, N., et al., *Measurements of carbonyl compounds around the Arabian Peninsula: overview and model comparison.* Atmospheric Chemistry and Physics, 2020. **20**(18): p. 10807-10829.
77. Colomb, A., et al., *Variation of atmospheric volatile organic compounds over the Southern Indian Ocean (30–49 S).* Environmental Chemistry, 2009. **6**(1): p. 70-82.
78. Karl, T., et al., *Use of proton‐transfer‐reaction mass spectrometry to characterize volatile organic compound sources at the La Porte super site during the Texas Air Quality Study 2000.* Journal of Geophysical Research: Atmospheres, 2003. **108**(D16).
79. Filella, I. and J. Penuelas, *Daily, weekly, and seasonal time courses of VOC concentrations in a semi-urban area near Barcelona.* Atmospheric Environment, 2006. **40**(40): p. 7752-7769.

80. MIYAKAWA, Y., S. KATO, and Y. KAJII, *Calibration of the Proton Transfer Reaction Mass Spectrometry (PTR-MS) Instrument for Oxygenated Volatile Organic Compounds (OVOCs) and the Measurement of Ambient Air in Tokyo.* Journal of Japan Society for Atmospheric Environment/Taiki Kankyo Gakkaishi, 2005. **40**(5): p. 209-219.
81. Gros, V., et al., *Volatile organic compounds sources in Paris in spring 2007. Part I: qualitative analysis.* Environmental chemistry, 2011. **8**(1): p. 74-90.
82. Gaimoz, C., et al., *Volatile organic compounds sources in Paris in spring 2007. Part II: source apportionment using positive matrix factorisation.* Environmental chemistry, 2011. **8**(1): p. 91-103.
83. Velasco, E., Pressley, S., Grivicke, R., Allwine, E., Coons, T., Foster, W, *Eddy covariance flux measurements of pollutant gases in urban Mexico City.* Atmospheric Chemistry and Physics, 2009. **9**(19): p. 7325-7342.
84. Herndon, S.C., et al., *Characterization of urban pollutant emission fluxes and ambient concentration distributions using a mobile laboratory with rapid response instrumentation.* Faraday Discussions, 2005. **130**(0): p. 327-339.
85. Jobson, B.T., et al., *On-line analysis of organic compounds in diesel exhaust using a proton transfer reaction mass spectrometer (PTR-MS).* International Journal of Mass Spectrometry, 2005. **245**(1): p. 78-89.
86. Knighton, W.B., et al., *Quantification of aircraft engine hydrocarbon emissions using proton transfer reaction mass spectrometry.* Journal of Propulsion and Power, 2007. **23**(5): p. 949.
87. Herndon, S.C., et al., *Hydrocarbon Emissions from In-Use Commercial Aircraft during Airport Operations.* Environmental Science & Technology, 2006. **40**(14): p. 4406-4413.
88. Akagi, S.K., et al., *Emission factors for open and domestic biomass burning for use in atmospheric models.* Atmos. Chem. Phys., 2011. **11**(9): p. 4039-4072.
89. Wisthaler, A., et al., *Organic trace gas measurements by PTR-MS during INDOEX 1999.* Journal of Geophysical Research: Atmospheres, 2002. **107**(D19): p. INX2 23-1-INX2 23-11.
90. Kolarik, B., et al., *The effect of a photocatalytic air purifier on indoor air quality quantified using different measuring methods.* Building and Environment, 2010. **45**(6): p. 1434-1440.
91. Vesin, A., et al., *Use of the HS-PTR-MS for online measurements of pyrethroids during indoor insecticide treatments.* Analytical and Bioanalytical Chemistry, 2012. **403**(7): p. 1907-1921.
92. Uhde, E. and N. Schulz, *Impact of room fragrance products on indoor air quality.* Atmospheric Environment, 2015. **106**: p. 492-502.
93. Schripp, T., et al., *Application of proton-transfer-reaction-mass-spectrometry for Indoor Air Quality research.* Indoor Air, 2014. **24**(2): p. 178-189.
94. Han, K.H., et al., *Determination of material emission signatures by PTR-MS and their correlations with odor assessments by human subjects.* Indoor Air, 2010. **20**(4): p. 341-354.
95. Cordell, R.L., et al., *Detection of chemical weapon agents and simulants using chemical ionization reaction time-of-flight mass spectrometry.* Analytical chemistry, 2007. **79**(21): p. 8359-8366.
96. Petersson, F., et al., *Real‐time trace detection and identification of chemical warfare agent simulants using recent advances in proton transfer reaction time‐of‐flight mass spectrometry.* Rapid Communications in Mass

Spectrometry: An International Journal Devoted to the Rapid Dissemination of Up‐to‐the‐Minute Research in Mass Spectrometry, 2009. **23**(23): p. 3875-3880.
97. Agarwal, B., et al., *Use of proton transfer reaction time-of-flight mass spectrometry for the analytical detection of illicit and controlled prescription drugs at room temperature via direct headspace sampling.* Analytical and bioanalytical chemistry, 2011. **400**(8): p. 2631-2639.
98. Jürschik, S., et al., *Rapid and facile detection of four date rape drugs in different beverages utilizing proton transfer reaction mass spectrometry (PTR‐MS).* Journal of mass spectrometry, 2012. **47**(9): p. 1092-1097.
99. Sabo, M., M. Malaskova, and Š. Matejčík, *Laser desorption with corona discharge ion mobility spectrometry for direct surface detection of explosives.* Analyst, 2014. **139**(20): p. 5112-5117.
100. Mayhew, C., et al., *Applications of proton transfer reaction time-of-flight mass spectrometry for the sensitive and rapid real-time detection of solid high explosives.* International Journal of Mass Spectrometry, 2010. **289**(1): p. 58-63.
101. González-Méndez, R.n., et al., *Enhancement of compound selectivity using a radio frequency ion-funnel proton transfer reaction mass spectrometer: improved specificity for explosive compounds.* Analytical chemistry, 2016. **88**(21): p. 10624-10630.
102. Sulzer, P., et al., *Applications of switching reagent ions in proton transfer reaction mass spectrometric instruments for the improved selectivity of explosive compounds.* International Journal of Mass Spectrometry, 2013. **354**: p. 123-128.
103. Baur, X., B. Poschadel, and L.T. Budnik, *High frequency of fumigants and other toxic gases in imported freight containers—an underestimated occupational and community health risk.* Occupational and environmental medicine, 2010. **67**(3): p. 207-212.
104. Wróblewski, T., et al., *Dissociation energies of protonated water clusters.* Radiation Physics and Chemistry, 2003. **68**(1-2): p. 313-318.
105. Wang, T., P. Španěl, and D. Smith, *Selected ion flow tube, SIFT, studies of the reactions of H_3O^+, NO^+ and $O2^+$ with eleven C10H16 monoterpenes.* Int. J. Mass Spec., 2003. **228**(1): p. 117-126.
106. Michel, E., et al., *A selected ion flow tube study of the reactions of H 3 O+, NO+ and O 2+ with methyl vinyl ketone and some atmospherically important aldehydes.* International Journal of Mass Spectrometry, 2005. **244**: p. 50-59.
107. Roach, J.A., et al., *Chromatographic separation and identification of conjugated linoleic acid isomers.* Analytica Chimica Acta, 2002. **465**(1-2): p. 207-226.
108. Ecker, J., et al., *A rapid GC–MS method for quantification of positional and geometric isomers of fatty acid methyl esters.* Journal of Chromatography B, 2012. **897**: p. 98-104.
109. Lacko, M., et al., *Addition of fast gas chromatography to selected ion flow tube mass spectrometry for analysis of individual monoterpenes in mixtures.* Atmospheric Measurement Techniques, 2019. **12**(9): p. 4965-4982.
110. Lacko, M., *Kinetic of Ion Molecular Ineraction Simulator (KIMI Sim)*. 2021: https://github.com/Progllar/KIMI-Simulator.
111. Runge, C., *Über die numerische Auflösung von Differentialgleichungen.* Mathematische Annalen, 1895. **46**(2): p. 167-178.

112. Spanel, P. and D. Smith, *Advances in on-line absolute trace gas analysis by SIFT-MS.* Current Analytical Chemistry, 2013. **9**(4): p. 525-539.
113. Španěl, P., Y. Ji, and D. Smith, *SIFT studies of the reactions of H3O+, NO+ and O2+ with a series of aldehydes and ketones.* International journal of mass spectrometry and ion processes, 1997. **165**: p. 25-37.
114. Dryahina, K. and P. Španěl, *A convenient method for calculation of ionic diffusion coefficients for accurate selected ion flow tube mass spectrometry, SIFT-MS.* International Journal of Mass Spectrometry, 2005. **244**(2-3): p. 148-154.
115. Španěl, P., K. Dryahina, and D. Smith, *A general method for the calculation of absolute trace gas concentrations in air and breath from selected ion flow tube mass spectrometry data.* International Journal of Mass Spectrometry, 2006. **249-250**: p. 230-239.
116. Hazra, M.K., J.S. Francisco, and A. Sinha, *Hydrolysis of glyoxal in water-restricted environments: formation of organic aerosol precursors through formic acid catalysis.* The Journal of Physical Chemistry A, 2014. **118**(23): p. 4095-4105.
117. Shkrob, I.A., et al., *Photoredox reactions and the catalytic cycle for carbon dioxide fixation and methanogenesis on metal oxides.* The Journal of Physical Chemistry C, 2012. **116**(17): p. 9450-9460.
118. Civiš, S., et al., *Photocatalytic transformation of CO2 to CH4 and CO on acidic surface of TiO2 anatase.* Optical Materials, 2016. **56**: p. 80-83.
119. Volkamer, R., U. Platt, and K. Wirtz, *Primary and secondary glyoxal formation from aromatics: experimental evidence for the bicycloalkyl− radical pathway from benzene, toluene, and p-xylene.* The Journal of Physical Chemistry A, 2001. **105**(33): p. 7865-7874.
120. Jang, M. and R.M. Kamens, *Characterization of Secondary Aerosol from the Photooxidation of Toluene in the Presence of NOx and 1-Propene.* Environmental Science & Technology, 2001. **35**(18): p. 3626-3639.
121. Tuazon, E.C., et al., *Yields of glyoxal and methylglyoxal from the nitrogen oxide (NOx)-air photooxidations of toluene and m-and p-xylene.* Environmental science & technology, 1984. **18**(12): p. 981-984.
122. Smith, D., T. Kleindienst, and C. McIver, *Primary product distributions from the reaction of OH with m-, p-xylene, 1, 2, 4-and 1, 3, 5-trimethylbenzene.* Journal of Atmospheric Chemistry, 1999. **34**(3): p. 339-364.
123. Yu, J., H.E. Jeffries, and R.M. Le Lacheur, *Identifying airborne carbonyl compounds in isoprene atmospheric photooxidation products by their PFBHA oximes using gas chromatography/ion trap mass spectrometry.* Environmental science & technology, 1995. **29**(8): p. 1923-1932.
124. Yu, J., H.E. Jeffries, and K.G. Sexton, *Atmospheric photooxidation of alkylbenzenes—I. Carbonyl product analyses.* Atmospheric Environment, 1997. **31**(15): p. 2261-2280.
125. Wroblewski, T., et al., *Ab initio and density functional theory calculations of proton affinities for volatile organic compounds.* European Physical Journal-Special Topics, 2007. **144**: p. 191-195.
126. NIST. *NIST WebBook Chemie, NIST Standard Reference Database Number 69*. Available from: http://webbook.nist.gov/chemistry/.
127. Mattioda, G. and A. Blanc, *Glyoxal*, in *Ullmann's Encyclopedia of Industrial Chemistry*. 2000.

128. Guimbaud, C., et al., *Kinetics of the reactions of acetone and glyoxal with O-2(+) and NO+ ions and application to the detection of oxygenated volatile organic compounds in the atmosphere by chemical ionization mass spectrometry.* International Journal of Mass Spectrometry, 2007. **263**(2-3): p. 276-288.
129. Stönner, C., et al., *Glyoxal measurement with a proton transfer reaction time of flight mass spectrometer (PTR‐TOF‐MS): characterization and calibration.* Journal of Mass Spectrometry, 2017. **52**(1): p. 30-35.
130. Lacko, M., et al., *Chemical ionization of glyoxal and formaldehyde with H_3O^+ ions using SIFT-MS under variable system humidity.* Phys. Chem. Chem. Phys., 2020.
131. Bohme, D., G. Mackay, and S.D. Tanner, *An experimental study of the gas-phase kinetics of reactions with hydrated hydronium (1+) ions (n= 1-3) at 298 K.* Journal of the American Chemical Society, 1979. **101**(14): p. 3724-3730.
132. Halden, R.U., *Plastics and health risks.* Annu Rev Public Health, 2010. **31**: p. 179-94.
133. Benjamin, S., et al., *A monograph on the remediation of hazardous phthalates.* J Hazard Mater, 2015. **298**: p. 58-72.
134. *DIRECTIVE 2005/84/EC OF THE EUROPEAN PARLIAMENT AND OF THE COUNCIL of 14 December 2005*. 2005: Official Journal of the European Union. p. 40-43.135.
135. EHCA – European Chemicals Agency, *Candidate List of Substances of Very High Concern of Authorisation*. 2022. Available from: http://echa.europa.eu/candidate-list-table/-/substance/
136. Shen, H.Y., *Simultaneous screening and determination eight phthalates in plastic products for food use by sonication-assisted extraction/GC-MS methods.* Talanta, 2005. **66**(3): p. 734-9.
137. Juhasz, M.L. and E.S. Marmur, *A review of selected chemical additives in cosmetic products.* Dermatol Ther, 2014. **27**(6): p. 317-22.
138. Sadeghi, G., E. Ghaderian, and A. O'Connor, *Determination of Dioctyl phthalate (DEHP) concentration in polyvinyl chloride (PVC) plastic parts of toothbrushes.* The Downtown Review, 2015. **1**(2).
139. Russo, M.V., et al., *Extraction and GC-MS analysis of phthalate esters in food matrices: a review.* RSC Adv., 2015. **5**(46): p. 37023-37043.
140. Jeilani, Y.A., B.H. Cardelino, and V.M. Ibeanusi, *Positive chemical ionization triple-quadrupole mass spectrometry and ab initio computational studies of the multi-pathway fragmentation of phthalates.* J Mass Spectrom, 2010. **45**(6): p. 678-85.
141. Michalczuk, B., et al., *Isomer and Conformer Selective Atmospheric Pressure Chemical Ionisation of dimethyl phthalate.* Physical Chemistry Chemical Physics, 2019.
142. Lacko, M., et al., *Ion chemistry of phthalates in selected ion flow tube mass spectrometry: isomeric effects and secondary reactions with water vapour.* Physical Chemistry Chemical Physics, 2020. **22**(28): p. 16345-16352.
143. Pysanenko, A., P. Španěl, and D. Smith, *Analysis of the isobaric compounds propanol, acetic acid and methyl formate in humid air and breath by selected ion flow tube mass spectrometry, SIFT-MS.* International Journal of Mass Spectrometry, 2009. **285**(1-2): p. 42-48.

144. Španěl, P., et al., *Breath acetone concentration; biological variability and the influence of diet.* Physiological measurement, 2011. **32**(8): p. N23.
145. Marschner, K., S. Musil, and J.i. Dědina, *Demethylation of Methylated Arsenic Species during Generation of Arsanes with Tetrahydridoborate (1−) in Acidic Media.* Analytical chemistry, 2016. **88**(12): p. 6366-6373.
146. Talmi, Y. and D. Bostick, *Determination of alkylarsenic acids in pesticide and environmental samples by gas chromatography with a microwave emission spectrometric detection system.* Analytical chemistry, 1975. **47**(13): p. 2145-2150.
147. Dedina, J. and D.L. Tsalev, *Hydride generation atomic absorption spectrometry*. Vol. 130. 1995: Wiley.
148. Dędina, J., *Generation of volatile compounds for analytical atomic spectroscopy.* Encyclopedia of Analytical Chemistry: Applications, Theory and Instrumentation, 2006.
149. Duben, O., et al., *Dielectric barrier discharge plasma atomizer for hydride generation atomic absorption spectrometry—Performance evaluation for selenium.* Spectrochimica Acta Part B: Atomic Spectroscopy, 2015. **111**: p. 57-63.
150. Kratzer, J., et al., *Atomization of As and Se volatile species in a dielectric barrier discharge atomizer after hydride generation: Fate of analyte studied by selected ion flow tube mass spectrometry.* Analytica Chimica Acta, 2022. **1190**: p. 339256.